Contributions to Mineralogy and Petrology (2021) 176:7
https://doi.org/10.1007/s00410-020-01757-2

ORIGINAL PAPER

Dual mixing for the formation of Neoproterozoic granitic intrusions within the composite Jiuling batholith, South China

Di Wang[1] · Xiao-Lei Wang[1]

Received: 24 February 2020 / Accepted: 4 November 2020

Abstract

Granite batholiths record the processes that occur during the formation and differentiation of the continental crust. The ~ 4000 km^2 composite Neoproterozoic Jiuling batholith is one of the largest batholiths in southern China and consists of four peraluminous granitoid intrusions that were emplaced at *ca.* 828–810 Ma. These granitoids define a trend that moves from the terrestrial towards the seawater Nd–Hf isotope array, indicating the source of these magmas incorporated increasing amounts of marine sedimentary material over time. Our new geochronological and geochemical data suggest that the composite Neoproterozoic Jiuling batholith formed incrementally via the intrusion of multiple batches of crustally derived melts. The intrusions within the batholith are characterized by decreasing Rb/Sr ratios and increasing Na/K ratios and $\varepsilon_{Hf}(t)$ values, suggesting variations in source composition over time. These inter-intrusion variations can be well explained by three-component mixing in magma sources (mature, immature sediments and felsic arc-related granitoids) prior to partial melting, with inter-sample variations within individual intrusions occurring as a result of the subsequent mixing of different melt batches. The first stage of mixing within the source of these magmas involves a significant variation in source compositions and cannot reflect the simple melting of a heterogeneous metasedimentary source region. The second stage of mixing occurred during magma ascent and storage, and is recorded by variations in mineral compositions (e.g., zircon). These inter-intrusion and inter-sample geochemical variations provide evidence that the peraluminous Jiuling batholith formed as a result of two mixing processes, namely mixing within the magma source region and mixing of multiple batches of granitic melts. This dual mixing could explain the significant geochemical diversity present within peraluminous granitoid rocks worldwide.

Keyword Dual mixing · Formation · Heterogeneous · Composite Jiuling batholith · Nd–Hf decoupling

Introduction

Understanding the formation and emplacement of composite granitic batholiths can provide significant insights into the processes involved in the formation of continental landmasses (e.g., Petford et al. 2000). Recent research has determined that these batholiths can form as a result of the incremental assembly of different magma batches, challenging previous models for the dynamics of, and processes involved in, composite batholith formation (e.g., Coleman et al. 2004; Glazner et al. 2004; Michel et al. 2008; Miller et al. 2011; Fiannacca et al. 2017). A single granitic intrusion can form over a short period of time (100 kyr–1 Myr), whereas the formation of a single batholith can extend over a time period of *ca.* 10 Myr (e.g., Coleman et al. 2004; Miller et al. 2011; Tichomirowa et al. 2019). This prolonged timespan could lead to larger geochemical variations amongst the different batches of magma that form a composite batholith, with these variations recorded as distinct changes in mineral chemistry. These variations also occur spatially, as evidenced by variations between different hand samples from a given single intrusion. The geochemical evolution of the magmas that form a batholith may also indicate changes in sources and magmatic processes amongst individual intrusions and/or batches of melts (e.g., Farner et al. 2014; Marsh

Communicated by Daniela Rubatto.

Electronic supplementary material The online version of this article (https://doi.org/10.1007/s00410-020-01757-2) contains supplementary material, which is available to authorized users.

✉ Xiao-Lei Wang
wxl@nju.edu.cn

[1] State Key Laboratory for Mineral Deposits Research, School of Earth Sciences and Engineering, Nanjing University, Nanjing 210023, China

Published online: 10 January 2021

2015; Nikkilä et al. 2016; Camilletti et al. 2020). More specifically, each batch of melt is generated over a very short period of time within a restricted area, meaning that mixing between different batches of magma is likely to be a common feature of batholith formation. The identification of this process provides further insights into the geochemical variations within granitic batholiths and the associated evolution of the continental crust.

Hafnium and neodymium isotopes can provide evidence of the processes involved in the petrogenesis of igneous rocks. Globally, Nd–Hf isotope data define two linear arrays, namely terrestrial (Vervoort et al. 1999) and seawater (Albarède et al. 1998) arrays. The seawater array diverges from the terrestrial array as a result of Nd–Hf decoupling, yielding an array of higher $^{176}Hf/^{177}Hf$ values relative to $^{143}Nd/^{144}Nd$ values that is rarely recorded in granitoids within the continental crust (Vervoort et al. 1999). This decoupling has been explained by models including the zircon effect of Patchett et al. (1984) and the garnet effect (Vervoort and Patchett 1996; Vervoort et al. 2000; Huang et al. 2017). However, even with these explanations, this decoupling still remains controversial (e.g., Vervoort and Blichert-Toft 1999; Vervoort et al. 1999, 2011; Van de Flierdt et al. 2007; Zheng et al. 2007; Stichel et al. 2012; Tang et al. 2014; Wang et al. 2018; Huang et al. 2019).

The composite Neoproterozoic Jiuling batholith crops out over an area of ~ 4,000 km^2 and is one of the largest granitic batholiths in southern China. It contains four separate Neoproterozoic intrusions (i.e. the Meiling, Jiuling, Shihuajian, and Jiuxiantang intrusions) that were emplaced sequentially, providing an ideal natural laboratory for research into the petrogenesis and evolution of voluminous peraluminous granitic batholiths. Although this area has been the focus of a significant amount of previous research (Li et al. 2003; Zhong et al. 2005; Wang et al. 2013c, 2018; Zhao et al. 2013; Xin et al. 2017; Rong et al. 2017, 2018), additional geochronological and geochemical data are required to constrain the formation of the peraluminous batholith as well as details of the magmatic processes that generated the geochemical diversity within the study area. This study presents new U–Pb and Hf isotope data for the Neoproterozoic intrusions within the batholith. The coupled bulk-rock and zircon isotope data for these intrusions record Nd–Hf decoupling that reflects the incorporation of marine sediments into the sources of the magmas that formed the batholith, indicating the strongly peraluminous composite Jiuling batholith records dual mixing processes, namely mixing of magma source material and mixing between different magma batches prior to and during their emplacement.

Geological background

The approximately E–W trending ~ 1500 km long Jiangnan Orogen (JO; Fig. 1a) divides the South China Block into the Cathaysia Block to the southeast and the Yangtze Block to the northwest (Wang et al. 2013a). The orogen is dominated by weakly metamorphosed Neoproterozoic sedimentary sequences and voluminous Neoproterozoic (860–800 Ma) magmatic rocks, both of which record the convergence history of the Yangtze and Cathaysia blocks (e.g., Wang et al. 2006).

The sediments within the JO have undergone low greenschist facies metamorphism and are divided into underlying and overlying sequences (Wang et al. 2013b). The underlying folded sequences have been previously described as "basement sequences" and include the widely distributed Shuangqiaoshan (SQS) Group within the eastern JO and the Sibao Group in the western JO. These units are thought to have formed in a back-arc basin associated with NW-dipping Neoproterozoic oceanic plate subduction beneath the Yangtze Block (e.g., Huang et al. 2003; Wang et al. 2007, 2012; Charvet 2013). The SQS Group has a total thickness of > 4 km and contains siltstone, slate, sandstone, greywacke, and conglomerate units (BGMRJX 1984). Detrital zircons from this group yielded U–Pb ages of *ca.* 845–815 Ma, constraining the maximum depositional ages of these sediments (Gao et al. 2008; Li et al. 2016).

The composite Jiuling batholith is located in the eastern part of the JO, along the southeastern margin of the Yangtze Block. It is split into the Meiling (~ 340 km^2), Jiuling (~ 3680 km^2), Shihuajian (~ 260 km^2), and Jiuxiantang (~ 44 km^2) intrusions. The Meiling and Jiuling intrusions were exclusively emplaced into the SQS Group units, whereas the Shihuajian and Jiuxiantang intrusions were emplaced into both the Jiuling intrusion and the SQS Group. The Jiuling, Shihuajian, and Jiuxiantang intrusions also commonly contain microgranular enclaves (Fig. 2). The Meiling, Jiuling, and Shihuajian intrusions are dominated by granodiorite and tonalite phases, with lesser amounts of monzogranite (Figs. 2, 3). All of these intrusions show porphyritic textures defined by K-feldspar and/or plagioclase phenocrysts that range in size from 2.5 to 10 mm and are hosted by a granitic matrix. The Meiling intrusion contains 40–55% plagioclase, 25–35% quartz, 10–15% K-feldspar, 5–15% biotite, 0–5% garnet, and minor amounts of accessory minerals. The Jiuling intrusion contains 35–55% plagioclase, 25–35% quartz, 5–15% K-feldspar, 5–15% biotite, 0–5% cordierite and 0–5% garnet. The Shihuajian intrusion is finer-grained than the Meiling and Jiuling intrusions, and contains 40–55% plagioclase, 5–40% K-feldspar, 25–35% quartz,

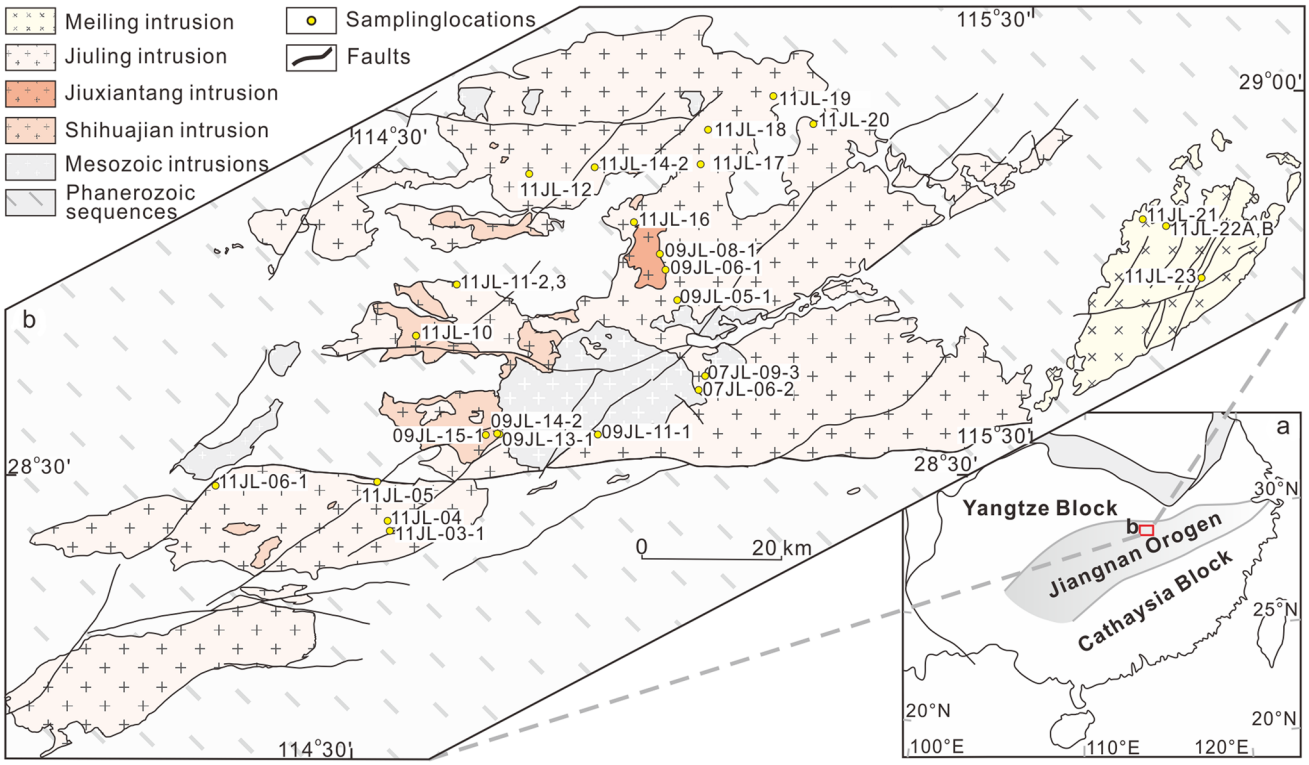

Fig. 1 Simplified geological map of the South China Block (**a**) and the composite Jiuling batholith (**b**) in the Jiangnan Orogen (modified after BGMRJX 1984; Wang et al. 2013a)

5–10% biotite, and 0–5% cordierite. The Jiuxiantang intrusion is dominated by a biotite tonalite phase, and contains 40–50% plagioclase, 25–35% quartz, 10–15% biotite and 2–7% K-feldspar. All of these Neoproterozoic intrusions contain accessory zircon, apatite, ilmenite and magnetite, and are classified as strongly peraluminous granites as evidenced by the presence of garnet and/or cordierite and the high aluminum saturation index (ASI) values (> 1.1). The Jiuling and Meiling intrusions were emplaced during the early stages of batholith formation as evidenced by (1) the spatial distribution of the intrusions, with the Meiling intrusion being spatially continuous with the Jiuling intrusion, (2) the similarity of the grainsizes, mineralogy, and lithologies within the two intrusions, (3) the geochemical similarities between the intrusions, including their rare earth element (REE) concentrations, and (4) the fact that the later-formed Shihuajian and Jiuxiantang intrusions were partly emplaced into the already-formed Jiuling intrusion.

Analytical methods

All analyses, including mineral and whole-rock geochemical and isotope analyses, were undertaken at the State Key Laboratory for Mineral Deposits Research, Nanjing University, Nanjing, China. Prior to analysis, zircons were separated using conventional heavy liquid and magnetic techniques before being imaged using transmitted and reflected light optical microscopy and cathodoluminescence (CL). The resulting images were used for spot selection for U–Th–Pb and Lu–Hf isotope analysis. Zircon U–Th–Pb isotope analysis was undertaken using laser ablation–inductively coupled plasma–mass spectrometry (LA–ICP–MS) employing an Agilent 7500a ICP–MS instrument coupled to a Geolas 193 nm LA system. A GJ-1 standard zircon (Jackson et al. 2004) was used as a primary standard for calibration with Mud Tank, Plešovice, and 91500 standard zircons used as validation reference

Fig.2 Representative outcrops of the Neoproterozoic intrusions in the composite Jiuling batholith. **a** the granodiorites of the Meiling intrusion; **b** granodiorites of the Jiuling intrusion; **c** microgranular enclaves in the Jiuling intrusion; **d** granodiorites of the Shihuajian intrusion; **e** the Jiuxiantang intrusion (tonalites) intruding into the Jiuling intrusion (granodiorites); **f** the boundary between the Jiuxiantang (bottom right) and Jiuling intrusions (top left)

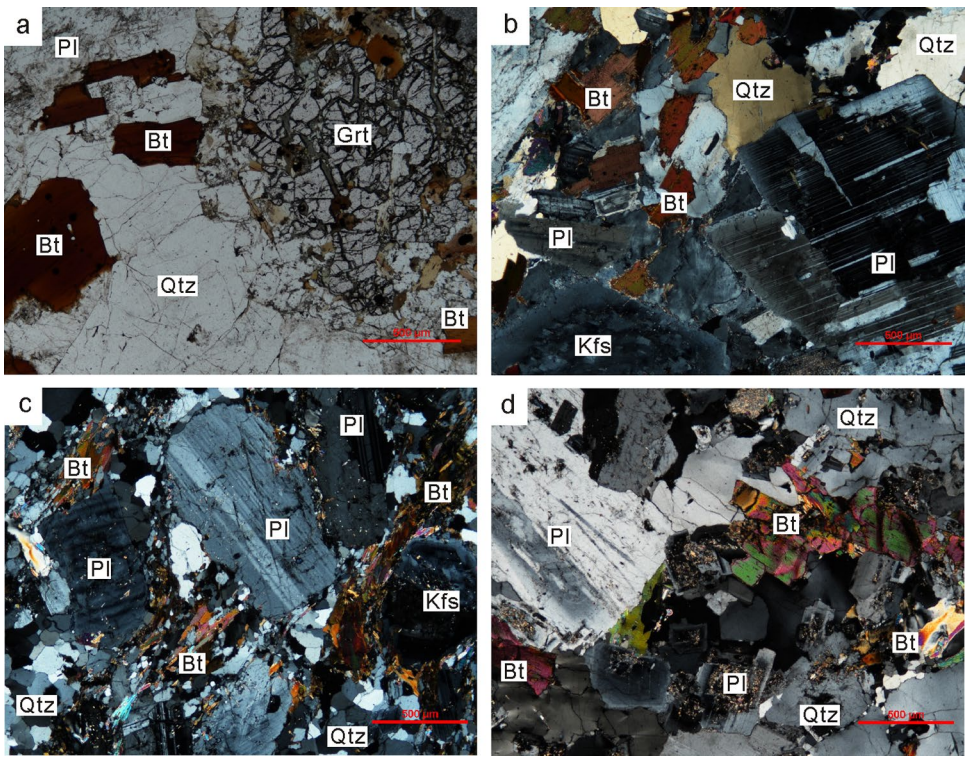

Fig. 3 Representative photomicrographs of the Neoproterozoic granitoids in the composite Jiuling batholith. **a**–**c** Granodiorite (sample 11JL-21, 11JL-04 and 09JL-13-1) from the Meiling, Jiuling and Shihuajian intrusion, respectively; and **d** tonalite (09JL-6-1) from the Jiuxiantang intrusion. Abbreviations are as follows: *Grt* garnet, *Pl* plagioclase, *Kfs* K-feldspar, *Bt* biotite, *Qtz* quartz

materials to monitor the accuracy and precision of the analyses. A NIST-612 glass standard was used for trace element concentration calibrations, employing ^{29}Si as an internal standard. The analytical processes used are similar to those outlined in Wang et al. (2017). Systematic sources of uncertainty [$^{206}Pb/^{238}U = 1.9\%$, $^{207}Pb/^{206}Pb = 1.3\%$ (2σ)] have been propagated into the final, calculated dates for each sample, as recommended by Horstwood et al. (2016).

In situ zircon Hf isotope analysis was undertaken in the same or similar domains as the U–Th–Pb analysis outlined above, using a GeoLas 193 nm ArF_3 laser ablation (LA) system attached to a Neptune Plus multicollector–ICP–MS (MC–ICP–MS) instrument. Routine analysis of the Mud Tank ($^{176}Hf/^{177}Hf = 0.282507 \pm 6$; Woodhead and Hergt 2005) and 91500 (Wiedenbeck et al. 1995) standard zircons were undertaken to ensure analytical accuracy. The analytical conditions and procedures used during this study are similar to those outlined in Griffin et al. (2000) and Wang et al. (2013a).

Whole-rock major element contents were determined by X-ray fluorescence using a Thermo Scientific ARL 9900 instrument yielding analytical precisions better than 2%. Whole-rock trace elements contents were determined using a Finnigan MAT Element II high resolution–ICP–MS (HR–ICP–MS) instrument following the procedures outlined in Gao et al. (2003), yielding analytical precisions that are generally better than 5%.

Results

Zircon U–Pb geochronology and Hf isotopes

The zircon grains analyzed during this study are colorless, and transparent with lengths of 50–200 μm. The majority are euhedral and prismatic to subhedral and contain weak to well-developed oscillatory zoning that is visible during CL imaging and is indicative of a magmatic origin. Only a few zircon grains are ellipsoidal with weakly developed oscillatory zoning (Fig. 4a–d). Some of the zircons exhibit multiple growth stages separated by intermittent phases of corrosion, as evidenced by the presence of corroded crystal outlines (Fig. 4b, c). In addition, some of these zircons have cores with different characteristics to the rest of the grain, such as variations in CL brightness or faint/oscillatory zoning. These cores yield older U–Pb dates (generally between the early Neoproterozoic and late Archean; see below), suggesting they are either inherited or xenocrystic. In comparison, zircon rims and those zircons without older cores yield uniformly younger ages. The results of U–Pb geochronology and Hf isotope analysis undertaken during this study are provided in Appendix 1.

The Meiling intrusion

Three samples (11JL-22A, 11JL-22B, and 11JL-23) from the Meiling intrusion were analyzed during this study, with zircons from these samples yielding Th/U values of 0.19–1.12. The youngest spot analyses yield $^{206}Pb/^{238}U$ ages between *ca.* 838 and *ca.* 799 Ma, and weighted average ages of 822 ± 10 Ma ($n = 14$; MSWD = 0.13), 817 ± 12 Ma ($n = 12$; MSWD = 0.07) and 827.9 ± 8.5 Ma ($n = 21$; MSWD = 0.09) for samples 11JL-22A, 11JL-22B and 11JL-23, respectively (Fig. 5a–c). All three of these weighted average ages are identical within uncertainty. The three inherited/xenocrystic grains (11JL-22A#04, #15; 11JL-22B#02) yield $^{207}Pb/^{206}Pb$ dates of 1752 ± 38, 1459 ± 51 and 1043 ± 121 Ma, respectively.

The Neoproterozoic magmatic zircon grains have initial $^{176}Hf/^{177}Hf$ ratios of 0.282220–0.282499, and the corresponding $\varepsilon_{Hf}(t)$ values that vary from −1.6 ± 1.1 to +8.9 ± 0.9 (Fig. 6). They also yield calculated T_{DM2} ages of 1.8–1.2 Ga. In contrast, the three inherited/xenocrystic zircons (11JL-22A#04, #15; 11JL-22B#02) have higher $\varepsilon_{Hf}(t)$ values (+3.6 ± 0.8, +11.3 ± 0.8 and +1.7 ± 0.8), with calculated T_{DM2} ages of 2.2, 1.5, and 1.8 Ga, respectively.

The Jiuling intrusion

Few of the zircon grains within these five Jiuling intrusion samples analyzed during this study (07JL-09–3, 11JL-04, 11JL-05-1, 11JL-11-3, and 11JL-18) have clear core–rim structures visible during CL imaging (Fig. 6). The zircon grains within these samples have a wide range of Th (47–1065 ppm) and U (157–2514 ppm) concentrations that yield Th/U ratios of 0.07–1.61 (generally 0.4–0.7). The youngest group of concordant analyses within each sample yield weighted mean $^{206}Pb/^{238}U$ ages of 817.5 ± 8.8 Ma ($n = 20$, MSWD = 0.10), 818 ± 12 Ma ($n = 13$, MSWD = 0.08), 827 ± 11 Ma ($n = 15$, MSWD = 0.06), 820 ± 12 Ma ($n = 15$, MSWD = 0.08) and 819 ± 14 Ma ($n = 11$, MSWD = 0.21), respectively (Fig. 5d–h). These ages are identical to each other within uncertainty. The remaining 13 older (inherited/xenocrystic) zircons yield ages from 2472 to 852 Ma.

The Neoproterozoic magmatic zircons yield initial $^{176}Hf/^{177}Hf$ ratios of 0.282048–0.282634, and a wide range of corresponding $\varepsilon_{Hf}(t)$ values and T_{DM2} ages of −7.7 ± 1.0–+13.6 ± 1.1 (Fig. 6) and 2.2–0.9 Ga, respectively. The inherited/xenocrystic zircons have $\varepsilon_{Hf}(t)$ values that range from −5.8 ± 1.0 to +10.6 ± 1.0 (Fig. 6) and calculated T_{DM2} ages of 3.3–1.5 Ga.

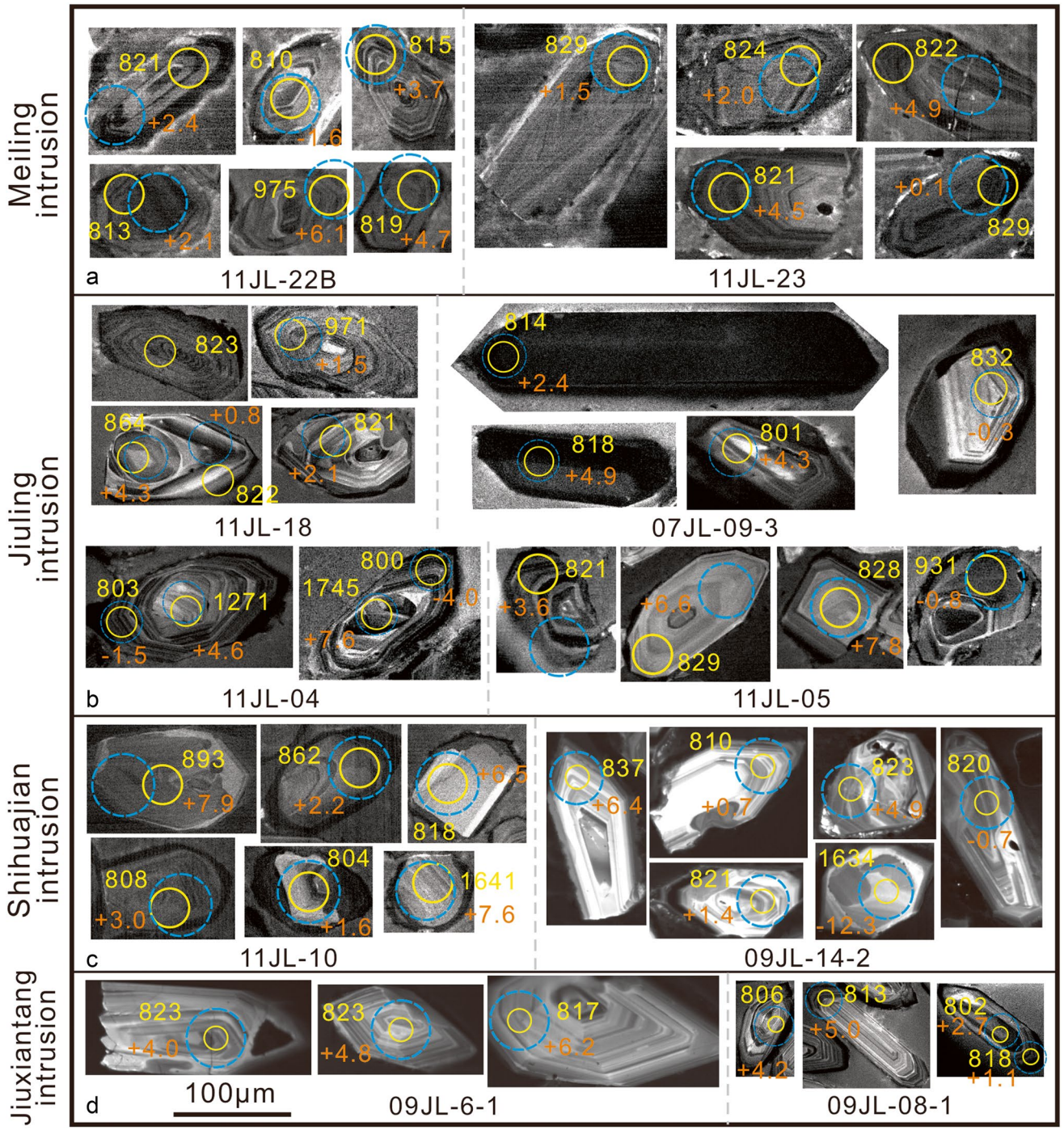

Fig. 4 Representative CL images showing the internal structure and morphology of zircons analyzed during this study. **a** granodiorite (sample 11JL-22B and 11JL-23) from the Meiling intrusion; **b** granodiorite (11JL-04, 11JL-5-1, 11JL-18 and 07L-09-3) from the Jiuling intrusion; **c** granodiorite (11JL-10 and 09JL-14-2) from the Shihuajian intrusion; and **d** tonalite (09JL-06-1 and 09JL-08-1) from the Jiuxiantang intrusion. Solid circles indicate the pits of U–Pb analyses and dashed circles indicate corresponding pits of Hf analyses; the U–Pb dates (Ma) and $\varepsilon_{Hf}(t)$ values for each analysis are shown near the circles

The Shihuajian intrusion

Zircons from the three samples of the Shihuajian intrusion analyzed during this study (09JL-13-1, 09JL-14-2, and 11JL-10) have Th/U ratios of 0.16–2.63 (generally 0.4–1.2). The youngest concordant zircons from these samples yield weighted mean $^{206}Pb/^{238}U$ ages of 820 ± 11 Ma ($n = 12$, MSWD = 0.92), 822 ± 10 Ma ($n = 14$, MSWD = 0.12) and

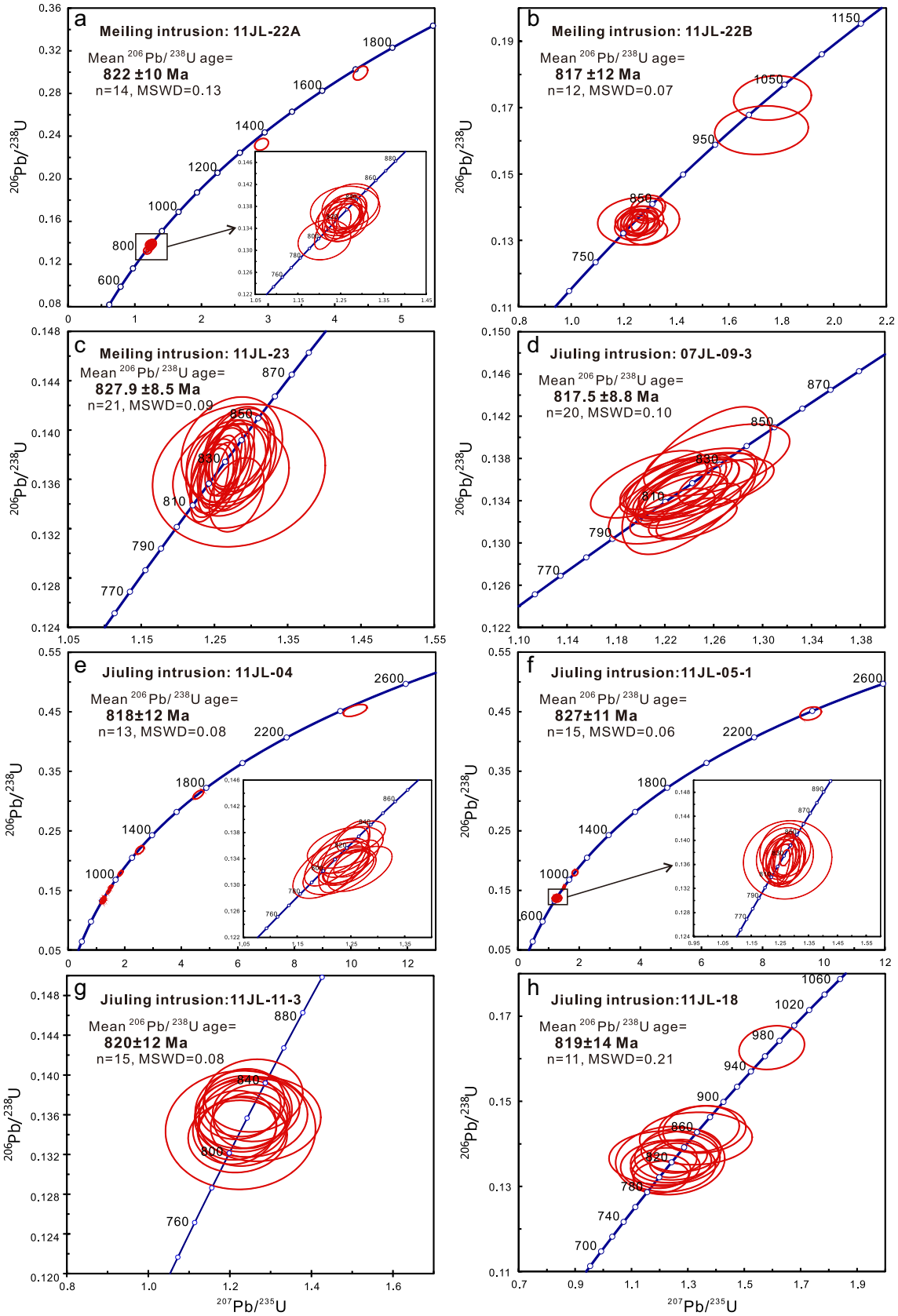

Fig. 5 Zircon LA–ICP–MS U–Pb concordia diagrams for Neoproterozoic granitoids of the composite Jiuling batholith

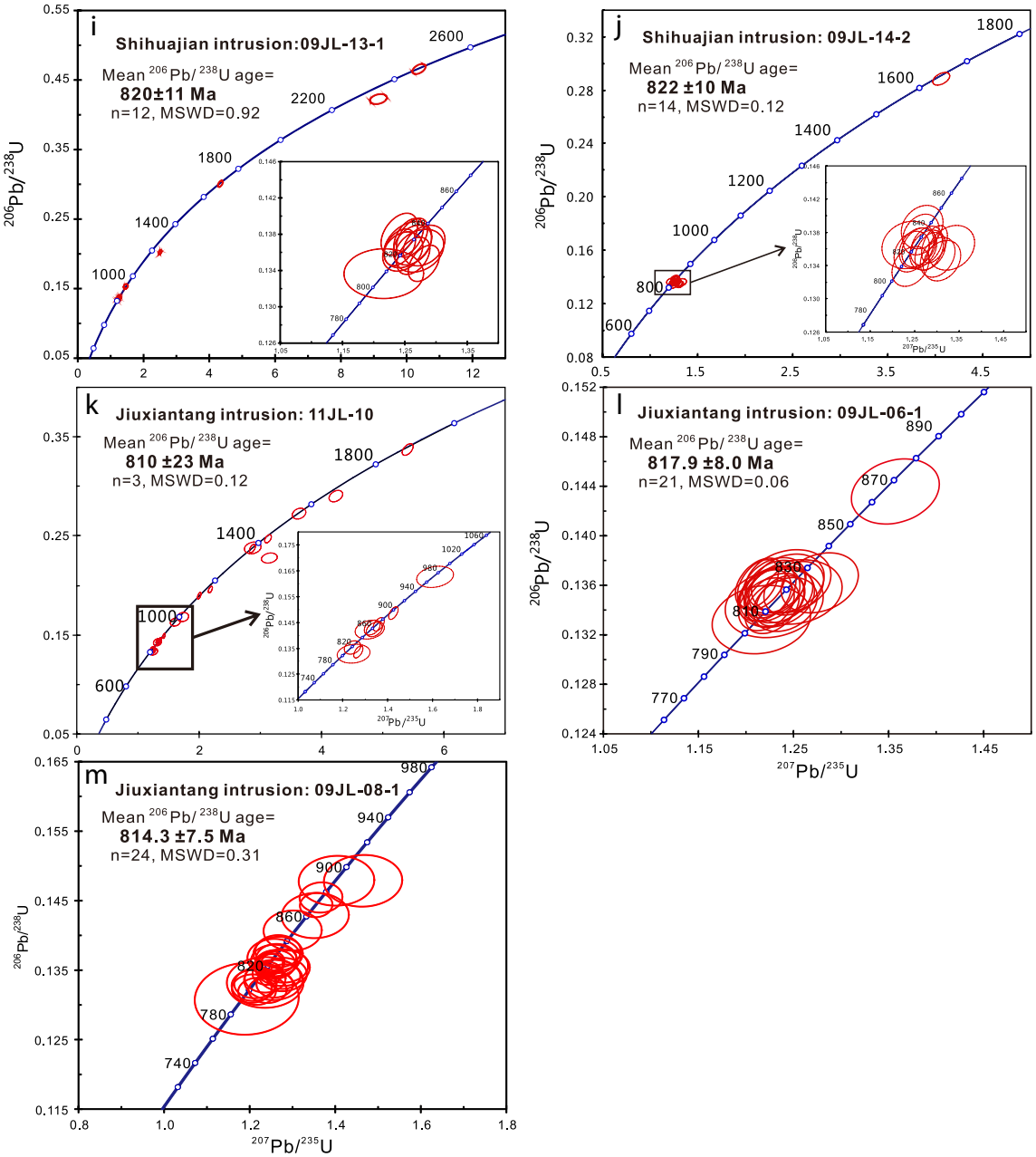

Fig. 5 (continued)

810 ± 23 Ma ($n = 3$, MSWD = 0.12), respectively (Fig. 5i–k). The remaining six inherited/xenocrystic zircon grains have old and concordant or near-concordant ages that range from 2472 ± 41 Ma to 857 ± 24 Ma.

All of the Neoproterozoic magmatic zircons within these three samples have initial $^{176}Hf/^{177}Hf$ ratios of 0.282220–0.282512, $\varepsilon_{Hf}(t)$ values from -1.2 ± 0.9 to $+9.1 \pm 0.9$ (Fig. 6), and T_{DM2} ages that range from 1.8 to 1.1 Ga. The inherited/xenocrystic zircons have $\varepsilon_{Hf}(t)$ values that vary from -12.3 ± 0.9 to $+11.5 \pm 1.0$, and T_{DM2} ages that range from 3.1 to 1.2 Ga.

The Jiuxiantang intrusion

The two samples from the Jiuxiantang intrusion analyzed during this study (09JL-06-1 and 09JL-8-1) contain zircons with Th/U rations of 0.08–0.97 (generally 0.3–0.7). The youngest spot analyses from samples 09JL-06-1 and 09JL-8-1 yield weighted mean $^{206}Pb/^{238}U$ ages of 817.9 ± 8.0 Ma ($n = 21$, MSWD = 0.06) and 814.3 ± 7.5 Ma ($n = 24$, MSWD = 0.31), respectively (Fig. 5l, m). Six spot analyses yield older and concordant ages from 889 ± 23 Ma to 849 ± 21 Ma.

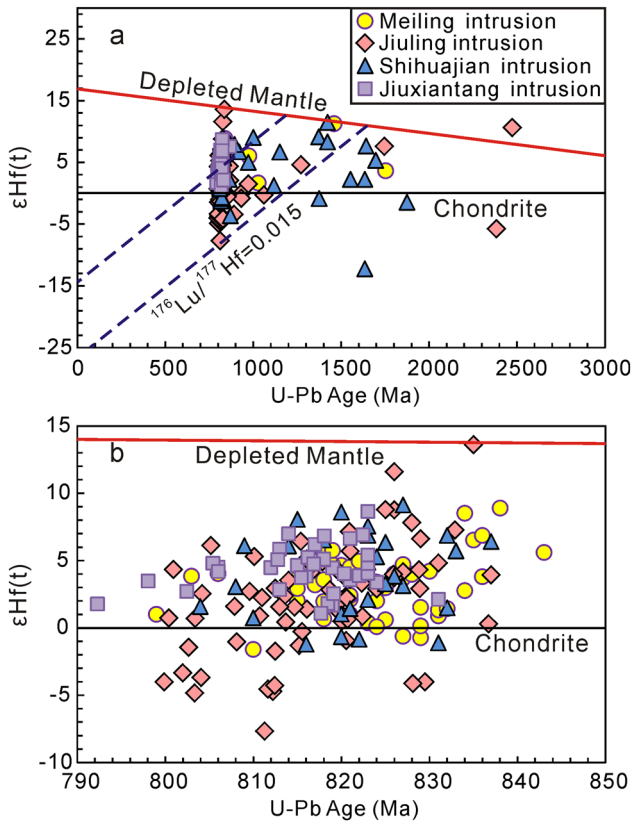

Fig. 6 $\varepsilon_{Hf}(t)$ vs. U–Pb age diagram for magmatic zircons in the Neoproterozoic intrusions. **a** is shown for the all analyses; **b** highlights the distribution of crystallizing zircon grains in (a)

The magmatic zircons in these samples have initial $^{176}Hf/^{177}Hf$ ratios of 0.282291 –0.282501, $\varepsilon_{Hf}(t)$ values that vary from $+1.1 \pm 1.0$ to $+8.6 \pm 0.9$ (Fig. 6), and two-stage Hf model ages that range from 1.7 to 1.1 Ga. A single inherited/xenocrystic zircon (09JL-06-1#19) yields an $\varepsilon_{Hf}(t)$ value of $+7.5 \pm 0.9$ and a T_{DM2} age of 1.3 Ga.

Geochemistry

Major elements

The Meiling granitoids contain restricted concentrations of SiO_2 (66.5–69.6 wt.%), TiO_2 (0.45–0.67 wt.%), MgO (1.25–1.90 wt.%), and total alkalis ($Na_2O + K_2O$; 6.01–6.70 wt.%), and have low Na_2O/K_2O ratios (0.64–0.78; Table 1 and Appendix 1). However, the granitoids from the Jiuling and Shihuajian intrusions contain more variable SiO_2 (62.4–74.7 wt.%), MgO (0.45–2.16 wt.%), CaO (0.56–3.65 wt.%; generally < 2.50 wt.%), and total alkali (3.51–8.10 wt.%; generally > 6.00 wt.%) concentrations in addition to more Na_2O/K_2O ratios (0.30–1.13, generally < 0.9 for the Jiuling granitoids and 1.11–1.13 for the Shihuajian granitoids; Fig. 7). In contrast, the Jiuxiantang granitoids contain 63.0–67.7 wt.% SiO_2 and have lower total alkali values (5.22–6.13 wt.%), higher CaO (2.70–3.31 wt.%) and MgO (1.73–2.95 wt.%) concentrations, and higher Na_2O/K_2O ratios (1.11–1.53) than the Meiling and Jiuling granitoids (Fig. 7). All of these granitoids are strongly peraluminous with aluminum saturation index [ASI = molar $Al_2O_3/(CaO + Na_2O + K_2O)$] values of 1.15–1.61, and have SiO_2 concentrations that negatively correlate with their TiO_2, Al_2O_3, $Fe_2O_3{}^T$, MnO, and MgO concentrations. The composite Jiuling batholith transitions from an early K-rich ($Na_2O/K_2O < 1$) and Ca-poor (CaO < 2.5 wt.%) phase to a late Na-rich ($Na_2O/K_2O > 1$) and Ca-rich (CaO > 2.5 wt.%) phase (Fig. 7), with the Shihuajian granitoids being transitional between these end-members. These data suggest that the granitoids record a change in source over time, as discussed below.

Trace elements

The Neoproterozoic granitoids contain variable trace element concentrations but are enriched in the light REE (LREE) relative to the heavy REEs (HREE; Appendixes 1, 2). The Meiling granitoids have $(La/Yb)_N$ values of 5.67–7.56 (where $_N$ denotes normalization to chondrite), negative Eu anomalies ($Eu/Eu^* = 0.55–0.63$, where $Eu^* = ½ \cdot [(Sm)_N + (Gd)_N]$), and high Rb/Sr ratios (1.66–3.55). In comparison, the Jiuling granitoids have variable Rb/Sr ratios (0.67–2.65, generally > 1.6) and REE concentrations with fractionated REE patterns [$(La/Yb)_N = 4.60–20.9$] and negative Eu anomalies ($Eu/Eu^* = 0.09–0.77$). The Shihuajian granitoids have relatively low Rb/Sr ratios (0.5–1.45) and similar REE patterns to the Jiuling granitoids, with $(La/Yb)_N$ values of 4.61–14.5. The Jiuxiantang granitoids are also similar to the Shihuajian granitoids in that they have low Rb/Sr ratios (0.49–0.90), fractionated REE patterns [$(La/Yb)_N = 4.79–8.57$], and negative Eu anomalies ($Eu/Eu^* = 0.58–0.78$). All of these granitoids have primitive mantle-normalized multi-element variation diagram patterns that are enriched in the light ion lithophile elements (LILE; Rb and Th) and the LREE, but are depleted in Nb, Ta, Sr, and Eu, indicating they are similar to arc-type granitoids (Zhou et al. 2002). These granitoids also record a systematic decrease in Rb/Sr ratios and REE contents from the early to the late stages of formation of the batholith.

Zircon saturation thermometry and Ti-in-zircon thermometry

Zircon saturation thermometry enables the estimation of zircon crystallization temperatures (T_{Zr}) if the whole-rock composition of a sample approximates the composition of a melt (e.g., Miller et al. 2003, 2007; Walker et al. 2007; Boehnke et al. 2013). This approach provides an

Table 1 A summary of petrological and geochemical information of the Neoproterozoic intrusions from the compsite Jiuling batholith

Intrusion	Sample	Rock type	MEs	Age (Ma)	Magmatic zircon εHf(t) range	Zircon εHf(t)[a]	2σ[a]	Whole-rock εNd(t)[a]	2σ[a]	SiO_2 (wt%)	ACNK	Na_2O/K_2O	GPS location	
Meiling	11JL-21	Granodiorite		828–817		0.7	1.2	−3.0	0.1	66.48	1.37	0.72	N 28°50′53.18 ″	E 115°40′15.78 ″
	11JL-22A	Granodiorite			−0.8 ~ +5.5	*3.0*	*1.1*	−2.2	0.1	67.90	1.35	0.73	N 28°50′11.74 ″	E 115°42′09.79 ″
	11JL-23	Granodiorite			+0.1 ~ +8.5	*3.5*	*1.0*	−2.6	0.1	69.56	1.50	0.64	N 28°46′24.20 ″	E 115°45′29.97 ″
Jiuling	07JL-06-2	Granodiorite	✓	827–817		2.9	1.4			65.55	1.44	0.54	N 28°36′59.0 ″	E 115°00′44.7 ″
	07JL-09-3	Granodiorite			−7.7 ~ +6.4	*3.0*	*1.3*	−3.3	0.1	69.18	1.41	0.60	N 28°38′06.5 ″	E 115°01′13.6 ″
	09JL-5-1	Granodiorite				3.4	0.8	−3.6	0.1	66.42	1.34	0.77	N 28°43′52.8 ″	E 114°58′44.6 ″
	09JL-11-1	Granodiorite				4.5	1.0	−1.7	0.2	69.40	1.20	1.75	N 28°33′23.8 ″	E 114°51′36.3 ″
	11JL-03-1	Granodiorite			−3.6 ~ +4.0	*0.4*	*1.4*	−3.2	0.1	67.29	1.46	0.65	N 28°25′49.35 ″	E 114°33′48.68 ″
	11JL-04	Granodiorite			−4.9 ~ +0.9	*−2.0*	*1.1*	−3.6	0.3	65.72	1.35	0.66	N 28°26′37.14 ″	E 114°33′34.48 ″
	11JL-06-1	Granodiorite				−1.4	2.0	−3.7	0.1	68.36	1.96	0.68	N 28°29′14.67 ″	E 114°18′37.36 ″
	11JL-11-2	Granodiorite				1.7	1.0	−3.7	0.3	70.70	1.40	0.88	N 28°45′06.89 ″	E 114°39′37.50 ″
	11JL-12	Granodiorite				2.7	0.7	−2.2	0.1	65.51	1.23	0.97	N 28°51′41.80 ″	E 114°45′52.46 ″
	11JL-14-2	Granite				5.9	1.0	−3.1	0.3	73.25	1.29	0.70	N 28°52′33.10 ″	E 114°51′40.56 ″
	11JL-16	Granodiorite				0.6	1.1	−2.5	0.1	65.36	1.55	0.58	N 28°49′54.36 ″	E 114°55′09.30 ″
	11JL-17	Granodiorite				-0.5	0.9	−2.8	0.1	70.78	1.34	0.66	N 28°52′34.85 ″	E 115°00′47.24 ″
	11JL-19	Granodiorite				3.2	2.2	−2.8	0.1	67.48	1.56	0.70	N 28°59′45.90 ″	E 115°07′23.05 ″
	11JL-20	Granodiorite				0.4	3.8	−3.4	0.3	66.80	1.25	1.13	N 28°57′26.51 ″	E 115°10′45.20 ″
Shihuajian	09JL-13-1	Granodiorite		822–810	−1.2 ~ +9.1	*4.6*	*2.2*	−2.3	0.1	63.38	1.19	1.45	N 28°33′31.6 ″	E 114°43′06.0 ″
	09JL-14-2	Granodiorite	✓		−1.2 ~ +8.6	*2.7*	*1.8*	−5.4	0.1	68.46	1.59	0.53	N 28°33′36.7 ″	E 114°42′55.5 ″
	09JL-15-1	Granodiorite				3.5	3.7	−4.3	0.1	69.17	1.61	1.01	N 28°33′30.2 ″	E 114°41′53.4 ″
	11JL-10	Granite			+1.6 ~ +6.5	*3.6*	*6.0*	−3.8	0.3	74.72	1.32	0.64	N 28°39′46.13 ″	E 114°36′07.05 ″
Jiuxiantang	09JL-06-1	Tonalite	✓	818–814	+1.7 ~ +8.6	*4.9*	*0.8*	−3.3	0.1	63.00	1.24	1.11	N 28°46′17.3 ″	E 114°57′41.9 ″
	09JL-08-1	Tonalite	✓		+1.1 ~ +6.9	*3.8*	*1.0*	−4.5	0.1	67.73	1.15	1.26	N 28°47′30.5 ″	E 114°57′03.9 ″

The data in italics are from this study

MEs microgranular enclaves, *SQS* Shuangqiaoshan

[a]The data of samples are from Wang et al. (2018)

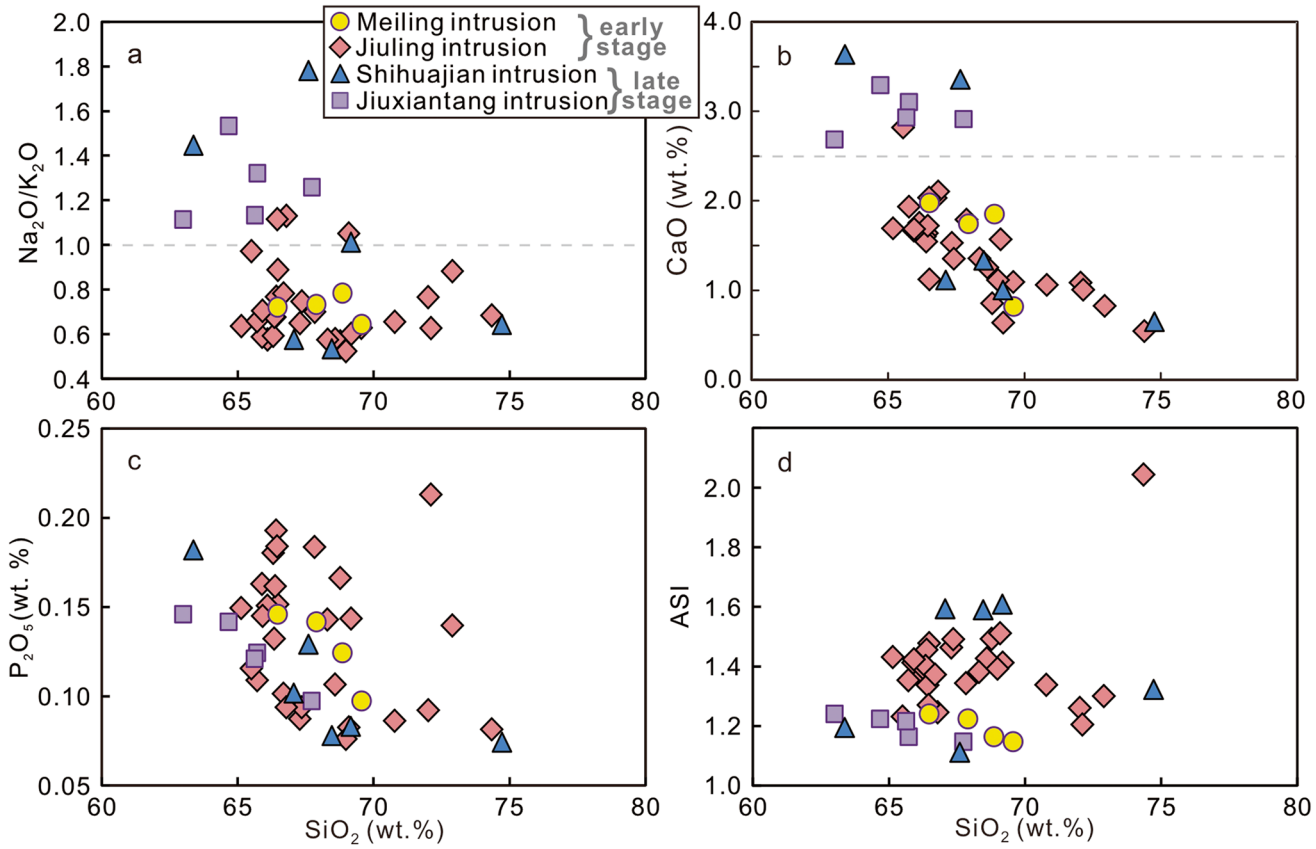

Fig. 7 **a**–**d** Diagrams showing the chemical variations of the Neoproterozoic granitoids

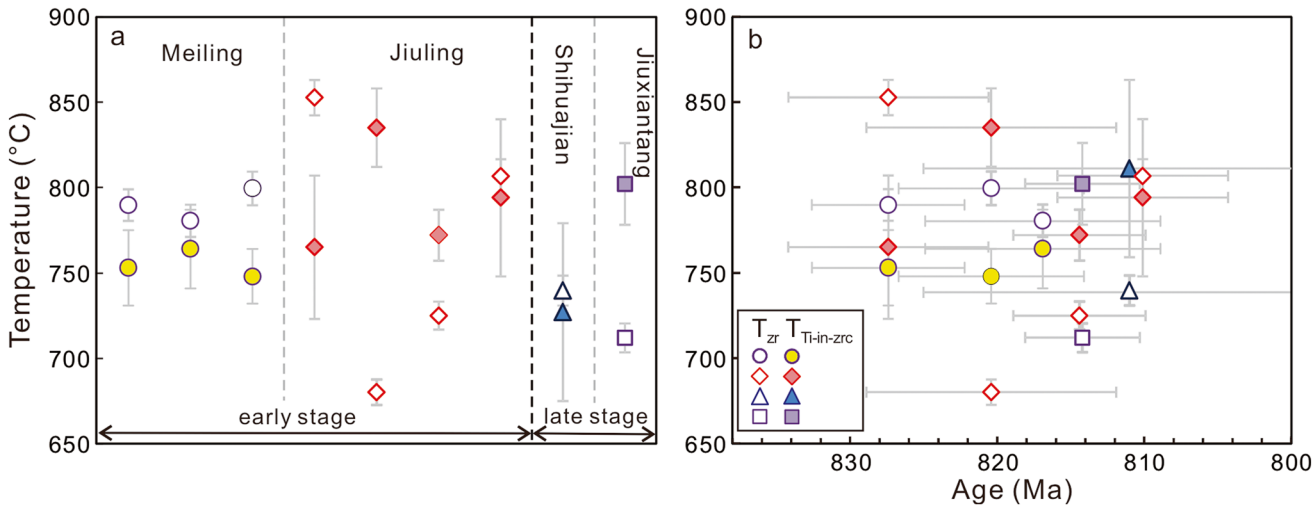

Fig. 8 Comparison of zircon saturation temperatures (T_{Zr}) and Ti-in-zircon temperatures ($T_{Ti\text{-}in\text{-}zrc}$) among the Neoproterozoic intrusions. Note: solid symbols for $T_{Ti\text{-}in\text{-}zrc}$ temperatures, and hollow symbols for T_{Zr} temperatures

estimate of the maximum or minimum melting temperature depending on whether the melt is zircon-saturated or not, respectively (e.g., Miller et al. 2003; Harrison et al. 2007). The Meiling granitoids have restricted T_{Zr} values (780 °C ± 9 °C–812 °C ± 10 °C; Fig. 8; Table 1 and Appendix 1) that contrast with the variable values obtained from the Jiuling intrusion (655 °C ± 7 °C–837 °C ± 10 °C). The Jiuxiantang granitoids have a narrow but low range of T_{Zr}

values (712 °C ± 8 °C–728 °C ± 9 °C), and the Shihuajian granitoids are intermediate between the other intrusions, yielding moderate T_{Zr} values from 712 °C ± 8 °C to 799 °C ± 9 °C. The fact that all of the samples from the study area—aside from the two dated samples from the Jiuling intrusion—contain inherited/xenocrystic zircon suggests that the majority of these magmas were zircon-saturated. This indicates that these temperatures represent maximum values as otherwise the inherited zircons within these samples would have dissolved within the melt.

Titanium-in-zircon thermometry provides an indication of the temperature of formation of natural zircons (e.g., Watson and Harrison 2005; Harrison et al. 2007; Hofmann et al. 2014). Apparent temperatures ($T_{Ti\text{-}in\text{-}zrc}$) calculated using this approach can also outline variations in temperature within magma chambers (Collins et al. 2016). The presence of Ti–rich accessory minerals can be used to constrain the Ti activity (a_{TiO2}) of a magmatic system to around 0.7 (e.g., Watson and Harrison 2005), enabling the calculation of $T_{Ti\text{-}in\text{-}zrc}$ values. The Meiling intrusion yields a restricted range of $T_{Ti\text{-}in\text{-}zrc}$ values (748 °C ± 16 °C–764 °C ± 23 °C), whereas the Jiuling intrusion yields a larger range of higher temperatures (765 °C ± 42 °C–835 °C ± 23 °C; Fig. 8; Table 1 and Appendix 1). However, the Shihuajian intrusion yields relatively low $T_{Ti\text{-}in\text{-}zrc}$ values (727 °C ± 52 °C) and the temperatures obtained from the Jiuxiantang intrusion (748 °C ± 14 °C) lie within the range of those obtained from the Meiling intrusion. This indicates that the early and late stage intrusions within the batholith record different temperature ranges. In addition, the magmatic system in the study area was not always zircon-saturated as two samples without xenocrystic cores yield higher $T_{Ti\text{-}in\text{-}zrc}$ values than T_{Zr} values, indicating that the intrusions in the study area formed from different melts.

Discussion

Sourcing of magmas within the composite Jiuling batholith

Granitoids form as a result of a number of different processes including partial melting of magma sources, magma mixing, fractionation, and other crystal mush processes during the evolution of the magmas within the system (e.g., Moyen and Laurent 2018; Rong et al. 2018). Regardless of the processes involved, the nature of the magma source exerts a first-order control on the composition of granitic melts. Moyen et al. (2017) collected and compared the compositions of more than 800 experimental granitic melts ($SiO_2 > 62$ wt.%) from diverse sources using a (Ca + Al) − Na + K + Al − 3 Al + 2 (Na + K) diagram, projected from biotite + quartz + H_2O. This diagram, which projects a number of tightly constrained arrays representing magmas derived from different sources (Fig. 9), enables the minimization of the effects of differentiation and can, therefore, be used to discriminate between granites derived from different sources (Moyen et al. 2017; Moyen and Laurent 2018).

The granitoids within the four Neoproterozoic intrusions that form the Jiuling batholith appear to be derived from different sources. The Jiuxiantang granitoid samples cluster along the Al = 3Ca + (Na + K) line (Fig. 9), and overlaps with the composition of experimental melts derived from felsic granitoids. In comparison, the Meiling, Jiuling, and Shihuajian granitoids define trends that are associated with more aluminous sources (e.g., immature and mature sediments). More specifically, the Jiuling granitoids plot close to the top of this diagram and define a steep slope that is indicative of the increased involvement of mature sedimentary material (e.g., pelites). However, samples from the Meiling and Jiuxiantang granitoids define more gentle slopes that

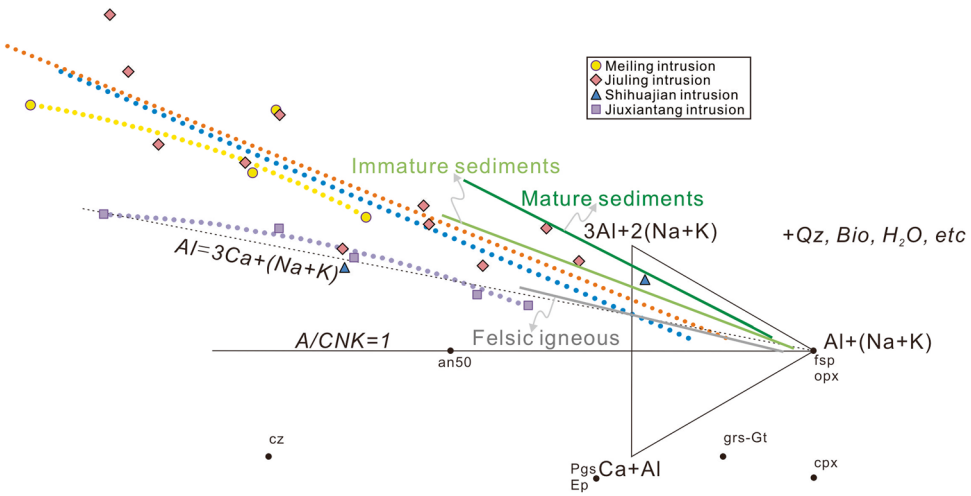

Fig. 9 Compositions of Neoproterozoic granitoids, projected from biotite on to the Ca + Al − 3Al + 2(Na + K) − Al + (Na + K) plane. The trends of immature sediments, mature sediments, and felsic igneous are modified according to Moyen et al. (2017). See Moyen et al. (2017) for details on the database and the projection

are indicative of the involvement of more immature sediments (e.g., sandstones). This suggests that these granitoids were derived from multiple different sources (e.g., felsic granitoids and immature and mature sediments) rather than a single heterogeneous crustal source region.

Zircon Hf–O isotopes and whole-rock Nd isotope data can also provide evidence on the nature of sources of granitoid magmas. The Neoproterozoic magmatic zircons within the intrusions in the study area have even more variable $\varepsilon_{Hf}(t)$ values (-7.7 ± 1.0–$+13.6 \pm 1.1$; Fig. 6). In comparison, the Neoproterozoic (*ca.* 850–795 Ma) detrital zircons within the SQS Group country rocks that surround these intrusions have variable $\varepsilon_{Hf}(t)$ values (-20.2–$+15.1$; Wang et al. 2013b; Li et al. 2016). Magmatic zircons within early Neoproterozoic arc-related granitoids (e.g., Xiqiu granitoids) of the Jiangnan Orogen have $\varepsilon_{Hf}(t)$ values that range from +6.9 to +12.6 (calculated for 820 Ma; Chen et al. 2009). The zircons within the Jiuling batholith have Hf isotope compositions that are similar to zircons within both the SQS Group and the Xiqiu granitoids. These magmatic zircons also yield T_{DM2} ages from 2.4 to 1.0 Ga (generally 2.0–1.1 Ga) that are similar to the range of T_{DM2} ages obtained for detrital zircons within the SQS Group (2.8–0.9 Ga; Wang et al. 2013b), suggesting the magmas that formed the batholith may have been derived from source material that was similar to the SQS Group. This is consistent with the similar Nd isotope compositions of the intrusions and the SQS Group (Wang et al. 2014), where the latter has $\varepsilon_{Nd}(t)$ values from −5.4 to +2.8 at *ca.* 820 Ma and Nd model ages of 2.4–1.3 Ga (Chen and Jahn 1998 and references therein). In comparison, the Neoproterozoic granitoids have similar calculated $\varepsilon_{Nd}(t)$ values and T_{DM2} ages from −5.4 to −1.9 and from 1.9 to 1.6 Ga (Wang et al. 2018), respectively. The majority of the magmatic zircons from the Jiuling batholith also yield $\delta^{18}O$ values > 7‰ (Wang et al. 2013c; Zhao et al. 2013) that are indicative of the presence of abundant supracrustal components within these magmas. Very few of these magmatic zircons have low $\delta^{18}O$ values (< 6‰; Appendix 3) that are indicative of the incorporation of minor amounts of material differentiated from mantle-derived melts (e.g., arc-related magmas) or the reworking of early arc-related intracrustal magmatic rocks. This indicates that the magmas that formed the Neoproterozoic granitoids in the study area were predominantly derived from supracrustal material (i.e., material geochemically similar to the SQS Group) with minor contribution from arc-related granitoids (e.g., the Xiqiu granitoids). Moreover, the volumes of the Meiling and Jiuling intrusions are much larger than that of the Shihuajian and Jiuxiantang intrusions, which could be related to different melting reactions for distinct source lithologies and/or different melt productivity.

Zircon cores can also provide information on the nature of the magma source of the magmas that formed the Jiuling batholith. These cores yield Archean–Neoproterozoic ages, and the majority (aside from sample 07JL-12-1) yield oxygen isotope compositional ranges with similar upper limits but lower limits that gradually decrease over time to match zircon rim compositions. This is illustrated by sample 11JL-19 from the Jiuling intrusion, which has $\delta^{18}O$ values of 5.60–10.3‰ and 8.46–10.6‰ for cores and rims, respectively, sample 09JL-13-1 from the Shihuajian intrusion with $\delta^{18}O$ values of 6.42–10.3‰ for cores and 5.84–9.74‰ for rims, and sample 09JL-08-1 from the Jiuxiantang intrusion, which has $\delta^{18}O$ values of 7.53–8.95‰ for cores and 7.72–9.33‰ for rims. The inherited zircons also have two-stage Hf model ages (T_{DM2}) that are broadly consistent with the T_{DM2} ages of the rims. This suggests that the compositions of these zircon cores reflect the compositions of the source of the host magma. These zircon cores record large inter-intrusion variations in O (up to 7.6‰ in $\delta^{18}O$ terms) and Hf isotopic ratios (Fig. 10) that are indicative of derivation from either different source rocks or a single, isotopically heterogeneous source. Inter-sample variations in zircon core oxygen isotope compositions are also indicative of the involvement of source materials formed by differentiation of mantle-derived magmas or by the reworking of pre-existing infracrustal materials (e.g., arc-related granitic magmas) and supracrustal crustal components (e.g., sediments).

The nature of the basement within the JO has been the focus of a significant amount of research but remains controversial. The 400 km long high-resolution seismic reflection profile reported by Dong et al. (2015) enabled the identification of an orogen buried beneath the Lengjiaxi

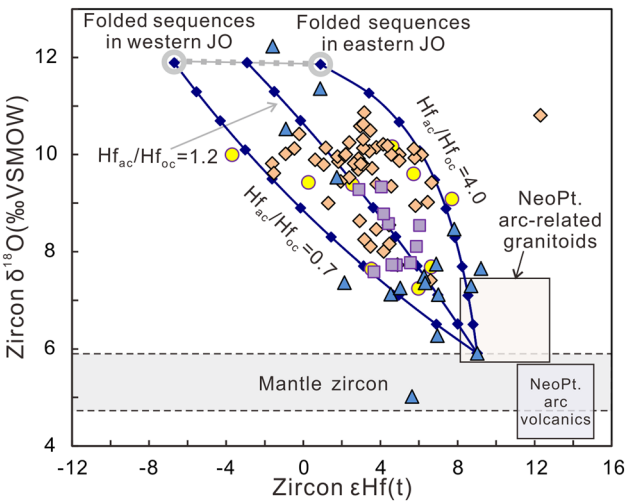

Fig. 10 Plot of $\delta^{18}O$ versus $\varepsilon_{Hf}(t)$ for zircons of these Neoproterozoic intrusions, suggesting multi-components mixing. The fields of Neoproterozoic arc-related granitoids and folded sequences in western and eastern JO are from Wang et al. (2013c). The oxygen isotopic data used in this publication can be found in the EarthChem Library (https://doi.org/10.26022/IEDA/111533)

Group (equivalent to the SQS Group) between the Yangtze and Cathaysia blocks. Dong et al. (2015) used this seismic data to suggest that this buried orogen formed during the Paleoproterozoic, which is consistent with the timing of *ca.* 2.0–1.85 Ga regional metamorphic and magmatic events (e.g., Yu et al. 2009, 2012). However, this buried orogen is likely to be compositionally and structurally similar and to have the same deformational history as an early Neoproterozoic arc terrane within the eastern segment of the JO. In addition, significant Neoproterozoic reworking throughout the whole Yangtze Block (Zhang et al. 2006a, b; Zhang and Zheng 2013) suggests that any Paleoproterozoic orogen may not have been preserved. It is likely that some ancient basement material (i.e., sedimentary sequences older than the Lengjiaxi and SQS Groups) could have been preserved during this orogenesis. This buried material may consist of arc-related granitoids that subsequently acted as a source for the magmas that formed the Neoproterozoic granitoids in the study area.

Combining these data with the information given above indicates that the first petrogenetic step in the formation of the Neoproterozoic Jiuling batholith was the mixing of material within the magma source region. Although a significantly heterogeneous source cannot be fully excluded, the compositional variations within the intrusions most likely record mixing within the source of these magmas. The geochemical data presented in this study, in particular the zircon Hf–O isotope data, provide evidence of three magma sources, namely arc-like felsic igneous rocks represented by early Neoproterozoic granitoids (913–905 Ma; Ye et al. 2007) in the eastern JO, and immature and mature supracrustal sources such as the folded sedimentary sequences in the western and eastern JO.

Magma mixing during formation of the composite Jiuling batholith

Magma mixing is thought to be involved in a number of different geological processes including the formation of the continental crust and the triggering of volcanic eruptions (Ruprecht and Bachmann 2010; Laumonier et al. 2014). It is often documented by field evidence, such as the presence of microgranular enclaves in plutonic systems (e.g., Barbarin 2005). The Neoproterozoic intrusions that form the Jiuling batholith contain common microgranular enclaves (Fig. 2). Magmatic zircon textures and geochemical compositions also record processes such as magma mixing (e.g., Laurent et al. 2017). Some of the zircons from the study area have complex internal textures that are suggestive of magma mixing (Fig. 4), and the combined titanium-in-zircon and zircon saturation thermometry discussed above also provide evidence of fluctuations in melt temperature (Tang et al. 2014), all of which suggests magma mixing. Linear geochemical trends in binary plots are often thought to provide evidence of mixing (e.g., Barbarin 2005; Clemens et al. 2016), and the Neoproterozoic granitoids in the study area define linear trends in binary major element diagrams (Fig. 7), again supporting the occurrence of magma mixing.

The large variations in the $\varepsilon_{Hf}(t)$ values of magmatic zircons from these Neoproterozoic intrusions (~7 epsilon units for the Jiuxiantang intrusion and > 10 epsilon units for the other intrusions) could be attributed to open system processes rather than just by the melting of heterogeneous crustal source(s) (e.g., Griffin et al. 2002; Yang et al. 2007; Appleby et al. 2010; Villaros et al. 2012) although magma mixing could also be involved (e.g., the mixing of crust- and mantle-derived magmas; e.g., Griffin et al. 2002; Belousova et al. 2006; Kemp et al. 2007). However, it is unlikely that this mixing involved mafic magmas for the following reasons. First, no contemporary mafic intrusions are associated with the Neoproterozoic granitoids in the study area. Second, the addition of mantle-derived magmas to form granitoids would increase the maficity ($MgO + FeO^T$) of the latter. This contrasts with the geochemistry of the Neoproterozoic granitoids, which record no such increase (Appendix 4). In addition, zircons with low oxygen isotope compositions (~6‰ $\delta^{18}O$; 11L-10#03, #06) are rare within the intrusions in the study area, and those that are present yield low $T_{Ti\text{-}in\text{-}zrc}$ values (~760 °C) that preclude the addition of mafic magmas during magma mixing. The magmatic zircons in the Neoproterozoic granitoids also have $\varepsilon_{Hf}(t)$ values that do not correlate with their Th/U values (Appendix 4b), again providing no evidence of mixing with mantle-derived magmas (Tang et al. 2014). Finally, the involvement of mafic magmas in the formation of these granitic rocks would have yielded a negative correlation between higher $\varepsilon_{Nd}(t)$ and zircon $\varepsilon_{Hf}(t)$ values and decreasing SiO_2 concentrations, a relationship which is not observed in the samples from the study area. All of these lines of evidence exclude the possibility that these granitoids formed as a result of magma mixing involving mantle-derived magmas.

Kemp et al. (2007) suggested that covariant ε_{Hf}–$\delta^{18}O$ arrays can be used to identify mixing and assimilation processes. The magmatic zircon rims from the Neoproterozoic granitoids in the study area span a wide range of values along the mixing lines ($Hf_{ac}/Hf_{oc} = 0.7$ and $Hf_{ac}/Hf_{oc} = 4.0$) present within this type of covariant ε_{Hf}–$\delta^{18}O$ array (Fig. 10). These large isotopic variations suggest that the intrusions record either the mixing of multiple batches of crustal partial melts or the assimilation of supracrustal rocks by mantle-derived mafic melts. Crustal contamination of a mantle-derived melt would require prohibitively large amounts of crustal components (60–70%) to explain the isotopic compositions of the Meiling and Jiuling granitoids. Thermal constraints considering the overall energy of the system also dictate that mantle-derived melts cannot

assimilate more than their own mass of crustal material. In addition, even if different degrees of partial melting of the same source material could produce different batches of magma, this type of melting would still produce isotopically homogenous magma batches. This contrasts with the highly variable range of zircon $^{176}Hf/^{177}Hf$ ratios present within individual Neoproterozoic intrusions in the study area. Each of these intrusions contains zircons with Hf isotope compositions that span between 4 and 14 epsilon units for the Meiling and Jiuling intrusions, 5–13 epsilon units for the Shihuajian intrusion, and 3–7 epsilon units for the Jiuxiantang intrusion. The presence of high and/or low $^{176}Hf/^{177}Hf$ outliers within these Neoproterozoic intrusions also suggests that the Neoproterozoic magmas that formed this batholith involved at least two melt batches of enriched and depleted $^{176}Hf/^{177}Hf$ melts. Villaros et al. (2012) suggested that the magmatic heterogeneity within a given batholith is inherited from the source of the magmas within the intrusion, potentially explaining any significant overlap between the ε_{Hf} values of magmatic zircons and the time evolved ε_{Hf} arrays of older inherited zircon cores with values calculated for the timing of crystallization of these inherited zircons. However, Farina et al. (2014) demonstrated that the dissolution of isotopically disparate inherited zircons during the emplacement of isotopically homogenous melts can generate late-stage Hf isotopic variability in the melt being emplaced and thus in any zircons forming from this melt. The modelling of Farina et al. (2014) also indicates that the extent of any Hf isotopic variability is dependent on how far below zircon saturation the melt was emplaced, the load of inherited zircons within the magma, and the cooling rate after emplacement. Nevertheless, there are documented cases where this isotopic variability is below analytical uncertainty because the melt was close to saturation when it was emplaced and/or the melt underwent rapid crystallization (e.g., Couzinié et al. 2017). Moreover, Farina et al. (2014) also demonstrated that even zircon under-saturated magmas undergoing slow cooling would generate only modest isotopic heterogeneity that would also be much smaller than the original isotopic heterogeneity of the inherited zircons. However, this research did not exclude the importance of magmatic processes such as magma mixing in the generation of small-scale isotope variability between zircons. The Neoproterozoic magmas in the study area must also have mixed thoroughly at some stage to yield relatively homogenous Hf isotope compositions, as evidenced by the presence of zircons with rims yielding intermediate $^{176}Hf/^{177}Hf$ ratios that lie between the Hf end-members of the distinct sources of the magmas. In summary, the large range of zircon $^{176}Hf/^{177}Hf$ values present in these granitoids provide robust evidence of magma mixing.

A change in the oxygen isotope composition of a magma can only be achieved by the addition of material with a distinct oxygen isotope composition (Valley 2003). This suggests that the presence of more than two apparent zircon $\delta^{18}O$ populations in the Neoproterozoic intrusions (Appendix 5) must represent mixing of at least two magmas. The majority of the zircons within the Meiling and Jiuling granitoids have rims and cores with resolvable variations in $\delta^{18}O$ values that vary from lower value cores to higher value rims, reflecting the mixing of a higher $\delta^{18}O$ melt with the original magma. However, some samples also document opposite trends (samples 11JL-21#15 and 16 from the Meiling intrusion; and samples 07JL-12-1#06 and 07, 11JL-16#01 and 02, 11JL-19#02 and 03, 11JL-19#07 and 08 from the Jiuling intrusion). This suggests that the system was open at the time of formation of these intrusions and underwent mixing of different batches of melt with different oxygen isotope compositions. In contrast, the Shihuajian and Jiuxiantang granitoids have zircons with $\delta^{18}O$ values that decrease from core to rim, reflecting mixing with lower $\delta^{18}O$ melts. This suggests that the batholith records a complex scenario where each individual intrusion formed from at least two melt batches, one high $\delta^{18}O$ and one lower $\delta^{18}O$, as evidenced by the by the highest and lowest measured zircon values for each intrusion (7.3‰ and 10.2‰ $\delta^{18}O$ melts for the Meiling intrusion, 7.4‰ and 10.9‰ $\delta^{18}O$ melts for the Jiuling intrusion, 5.0‰ and 13.1‰ $\delta^{18}O$ melts for the Shihuajian intrusion, and 7.6‰ and 9.3‰ $\delta^{18}O$ melts for the Jiuxiantang intrusion). These large variations in zircon oxygen isotope compositions suggest that the intrusions record the mixing of multiple batches of evolved magma that had undergone zircon crystallization, indicating that this mixing occurred during magma ascent and storage.

In summary, the Neoproterozoic intrusions in the study are the result of two stages of mixing within the magma source and during magma storage and ascent. The first stage occurred in the granitoid source region and involved the mixing of immature and mature sedimentary and arc-related granitoid sources, and the second stage involved different melt batches, as evidenced by the variable zircon Hf–O isotope compositions observed in the intrusions and the linear correlations present between major element concentrations within samples from the study area.

Nd–Hf decoupling and "seawater array" granitoids

It is well known that Lu–Hf and Sm–Nd isotopes behave in a covariant manner during magmatic processes (e.g., Vervoort and Blichert-Toft 1999; Vervoort et al. 1999). However, the majority of Neoproterozoic granitoids scatter away from "the terrestrial array" of Vervoort et al. (1999), providing evidence of Nd–Hf decoupling (Fig. 11a). Four main processes can cause this decoupling: (1) an abnormal enrichment in radiogenic Hf isotopes, a process that occurs in long-lived, fluid-dominated arc systems (e.g., Polat and

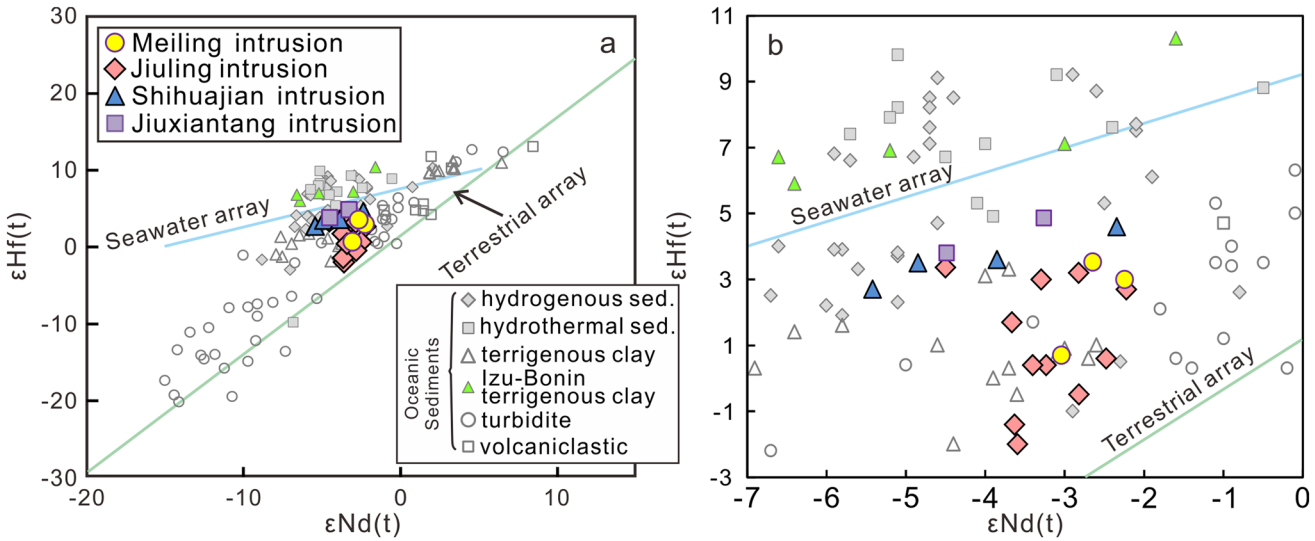

Fig. 11 Diagrams showing variations in (**a**, **b**) $\varepsilon_{Nd}(t)$ vs. $\varepsilon_{Hf}(t)$ for the Neoproterozoic granitoids and marine sediments worldwide. Note: the "terrestrial array" and "seawater array" are modified after Albarède et al. (1998), Vervoort et al. (1999), Carpentier et al. (2009) and Vervoort et al. (2011) and references therein. Nd and Hf isotopic compositions of marine sediments from Vervoort et al. (2011) and references therein

Münker 2004; Janney et al. 2005; Zheng et al. 2007); (2) high-grade metamorphism and partial melting of the lower crust (Vervoort et al. 2000; Schmitz et al. 2004); (3) the "zircon effect" (e.g., Patchett et al. 1984; Carpentier et al. 2009; Tang et al. 2014); and (4) the "garnet effect" (Vervoort and Patchett 1996; Vervoort et al. 2000; Huang et al. 2017). The latter both affect sources during non-modal melting with respect to zircon and garnet, respectively, generating out of equilibrium melt–source compositions as discussed below.

The tetrad effect ($TE_{1,3}$) can be used to identify the effects (or the segregation) of magmato-hydrothermal fluids (e.g., Irber 1999), where granitic samples with low Nb/Ta ratios (< 5) are most likely to have undergone significant chemical modification during fluid–rock interaction (Ballouard et al. 2016). The Neoproterozoic granitoids have whole-rock $TE_{1,3}$ values of 0.98–1.21 (generally < 1.10) and Nb/Ta ratios of 3.8–13.9 (generally > 8), both of which preclude the possibility of fluid interaction. All of these granitoids also have variable Lu/Hf ratios that do not correlate with their $\varepsilon_{Hf}(t)$ values, indicating that this isotopic decoupling cannot be controlled by high Lu/Hf ratios. The Neoproterozoic granitoids have also not undergone high-grade metamorphism, contain zircons with high Th/U (generally > 0.4) values and oscillatory zoning visible under CL imaging, have low Nb/U ratios (< 7.27 versus ~ 4.5 for the upper crust and ~ 25 for the lower crust; Rudnick and Gao 2003), and were emplaced at low pressures (< 0.2 GPa; BGMRJX 1984). These observations suggest that the granitoids cannot have been subject to high-grade metamorphism or partial melting within the lower crust. The presence of garnet during partial melting generates melts with elevated REE concentrations, Lu/Hf ratios, and $\varepsilon_{Hf}(t)$ values, which is contrary to the results from the granitoids in the study area; this implies that the Nd–Hf decoupling identified in this study cannot have been the result of any of these processes. The final possibility is the "zircon effect", which relies on the facts that zircon is very resistant to chemical alteration, and that Zr and Hf are both concentrated within the zircon that tends to be deposited in coarse-grained detrital sediments (Patchett et al. 1984). This means that zircon-bearing sandy sediments have very low Lu/Hf values, and clay-poor sandstones have low Lu/Hf values, meaning that it is difficult to significantly change the Hf isotope composition of a sediment without involving detrital zircons (Carpentier et al. 2009). Zircon abundances within magma sources can be estimated using whole-rock Zr concentrations. The studied samples record a negative relationship between whole-rock Zr concentrations and $\varepsilon_{Hf}(t)$ values. In addition, the majority of inherited zircon cores have more negative $\varepsilon_{Hf}(t)$ values (calculated for the timing of crystallization) than their rims, indicating that the presence of these zircons within the source rocks for the magmas that formed the Jiuling batholith would have decreased the $\varepsilon_{Hf}(t)$ values of the granitoids shown in Fig. 11b. This suggests that the zircon effect may explain the isotopic decoupling observed within the studied samples.

The above discussion indicates that the mixing of magmas with abnormally high $\varepsilon_{Hf}(t)$ values generated by the zircon effect caused the Nd–Hf decoupling in the study area. Microgranular enclaves are very common within the Neoproterozoic intrusions (Fig. 2), as evidenced by samples 09JL-06-1 and 09JL-08-1 from the Jiuxiantang intrusion and sample 09JL-14-2 from the Shihuajian intrusion.

All of these samples contain microgranular enclaves that may have formed during the mixing of melts with predominantly supracrustal origins (e.g., Zhao et al. 2013). As discussed above, magma mixing is likely to have been an important process in the formation of these Neoproterozoic granitoids; however, all of the granitoids with microgranular enclaves record Nd–Hf decoupling, and the presence of these enclaves provides direct evidence of variations in the degree of mixing. Further studies on these microgranular enclaves are needed to provide more information on this isotopic decoupling, although this is outside the scope of this study. It is likely that the source of the magmas in the study area contained marine sediments (e.g., terrigenous clays). These marine sediments have elevated $\varepsilon_{Hf}(t)$ values relative to their $\varepsilon_{Nd}(t)$ values, and contain zircons with high oxygen isotope values (e.g., Vervoort et al. 2000; Valley et al. 2005), characteristics that are also present within the Shihuajian and Jiuxiantang granitoids. More specifically, five types of marine sediments (i.e., turbidites, terrigenous clays, and volcaniclastic, hydrothermal and hydrogenetic sediments) can be distinguished using lithological and geochemical variations (Vervoort et al. 2011). Terrigenous clay, hydrothermal and hydrogenetic sediments plot closer to the "seawater array" than the other sediments, and are proximal to the Neoproterozoic granitoid samples analyzed during this study (Fig. 11). These granitoids have Nd/Hf values < 6, consistent with the composition of terrigenous clays. The geochemical characteristics outlined above are also inconsistent with derivation from hydrothermal and hydrogenetic sedimentary sources. For example, terrigenous clays within the Izu-Bonin region plot above the "seawater array" (Fig. 11), indicating they cannot have been present in the source of the Neoproterozoic granitoids in the study area. The granitoids were most likely derived from magmas generated by the partial melting of sedimentary material within the eastern and western JO (e.g., the SQS and Sibao Groups) that are thought to have originally been marine sediments deposited in a back-arc basin associated with oceanic subduction (Wang et al. 2012; Charvet 2013). In conclusion, melts derived from marine sediments (e.g., terrigenous clays) have high $\varepsilon_{Hf}(t)$ values as a result of the zircon effect associated with this type of source material, with the mixing of these magmas accounting for the Nd–Hf decoupling observed in the study area.

Magma construction mechanism

The concept of intrusions as large ascending molten blobs (also termed magma chambers) remains widespread in the geological community and commonly guides the interpretation of field data (e.g., Bateman 1992; Clarke 1992). A contrasting view is that the diapiric ascent of magma is too slow and energetically inefficient to be geologically significant, meaning that large magma bodies only form when they are continually fed by dikes during emplacement (e.g., Petford et al. 2000). However, this is contrary to new geochronological and geophysical data that indicate that large intrusions can accumulate incrementally over millions of years (e.g., Coleman et al. 2004; Glazner et al. 2004; Chambers et al. 2020). The intrusions that form the focus of this study also provide evidence that batholiths can form from multiple batches of magma with distinct geochemical characteristics.

The Meiling and Jiuling intrusions were emplaced into wall rocks of the SQS Group and were subsequently intruded by the Shihuajian and Jiuxiantang intrusions, with the ages of these distinct intrusive phases being identical within uncertainty. The Meiling and Jiuling intrusions formed during the early stages of batholith development and are lithologically similar, dominated by medium- to coarse-grained granodiorites and tonalites. These two intrusions have low Na_2O/K_2O ratios (generally < 1.0), contain low concentrations of CaO (generally < 2.5 wt.%), and have high Rb/Sr ratios (generally > 1.6), which indicates they formed from magmas derived from similar sources. However, the two intrusions also have some geochemical differences and the Jiuling granitoids yield higher and more variable temperatures than those recorded within the Meiling granitoids. The Jiuling intrusion also contains zircons with a broader range of zircon $\delta^{18}O$ (7.3–10.9‰) and $\varepsilon_{Hf}(t)$ (−7.7–+13.6) values and has a wider range of $\varepsilon_{Nd}(t)$ values (+1.0–+5.0) than the Meiling intrusion ($\delta^{18}O$: 9.1–10.2%; $\varepsilon_{Hf}(t)$: −1.6–+8.9; $\varepsilon_{Nd}(t)$: +2.7–+3.6; Wang et al. 2018 and this study). The large inter-intrusion variations in zircon Hf–O isotopes and whole-rock Nd isotopic compositions also indicate these intrusions formed from magmas derived from distinctly different sources. The highly variable zircon Hf–O isotope compositions recorded by single samples from these intrusions ($\delta^{18}O$: up to 3.4‰; $\varepsilon_{Hf}(t)$: up to 13 epsilon units) indicate the Meiling and Jiuling intrusions formed as a result of the mixing of multiple batches of magma generated by variable extents of disequilibrium melting.

The Shihuajian intrusion is markedly different from the Meiling and Jiuling intrusions in a number of respects. The Shihuajian intrusion was emplaced into the Jiuling intrusion, although both contain fine-grained granodiorites and tonalites and formed during the late stages of batholith genesis. The Shihuajian granitoids also have lower Rb/Sr ratios (< 1.6) and more variable Na_2O/K_2O ratios (from > 1.0 to < 1.0) and CaO concentrations (0.66–3.65 wt.%) than the Jiuling intrusion. The Shihuajian granitoids also records lower magmatic temperatures, contain more abundant inherited/xenocrystic zircons, and contain zircons with rims that have a wider range of $\delta^{18}O$ values (5.0–13.1‰; Appendix 1), but similar $\varepsilon_{Hf}(t)$ values (−1.2–+9.1) than those within the Meiling intrusion. The Shihuajian intrusion also records larger variations in zircon Hf–O isotope and whole-rock geochemical compositions than the earlier intrusions, indicating that this phase of batholith

formation involved a different magma source than that which generated the Meiling and Jiuling intrusions. This phase of batholith formation must have involved the mixing of multiple batches of magma with different geochemical compositions, as reflected by the inter-sample range of zircon isotopic ($\delta^{18}O$: up to 8.1‰; $\varepsilon_{Hf}(t)$: up to 13 epsilon units) and whole-rock geochemical compositions obtained from samples of the Shihuajian granitoids.

The Jiuxiantang intrusion was emplaced into the Jiuling intrusion and also represents the late phase of batholith formation. However, this intrusion is dominated by a biotite tonalite phase and has low Rb/Sr ratios (< 1.0), high Na_2O/K_2O ratios (> 1.0) and high concentrations of CaO (> 2.5 wt.%; Fig. 7). Magmatic zircons within this intrusion yield low $T_{Ti\text{-}in\text{-}zrc}$ temperatures and a restricted range of high $\varepsilon_{Hf}(t)$ values (+ 1.1 – + 8.6), but relatively low $\delta^{18}O$ values (7.6–9.3‰; Appendix 1). This intrusion is also free of inherited/xenocrystic zircons. Both the later Shihuajian and Jiuxiantang granitoids also have Nd and Hf isotope compositions that lie closer to the "seawater array" than the other intrusions within the batholith. The large inter-intrusion and inter-sample variations in zircon Hf–O isotopes and whole-rock major and trace element compositions also provide robust evidence of mixing in the source for the Shihuajian magmas as well as mixing of magma batches during ascent and storage prior to emplacement.

The field relationships and lithological, geochemical, and geochronological data outlined during this study indicate that the composite Jiuling batholith accumulated incrementally, despite the fact that the age of the different intrusions within the batholith are indistinguishable within uncertainty. The detailed discussion of the processes involved in this incremental accumulation is beyond the scope of this study; however, large inter-intrusion variations in zircon Hf–O isotope and whole-rock major and trace element compositions provide evidence of derivation from different magma sources. Variable zircon Hf and O isotope compositions within individual intrusions also provide evidence of the mixing of multiple batches of magma generated by variable extents of disequilibrium melting during the evolution of the magmas that formed these intrusions (Fig. 12). All of this indicates that the geochemical variations within the Neoproterozoic intrusions and within individual samples from these intrusions reflect the mixing of three components within the sources for these magmas and the mixing of different geochemically distinct batches of magma during ascent and storage.

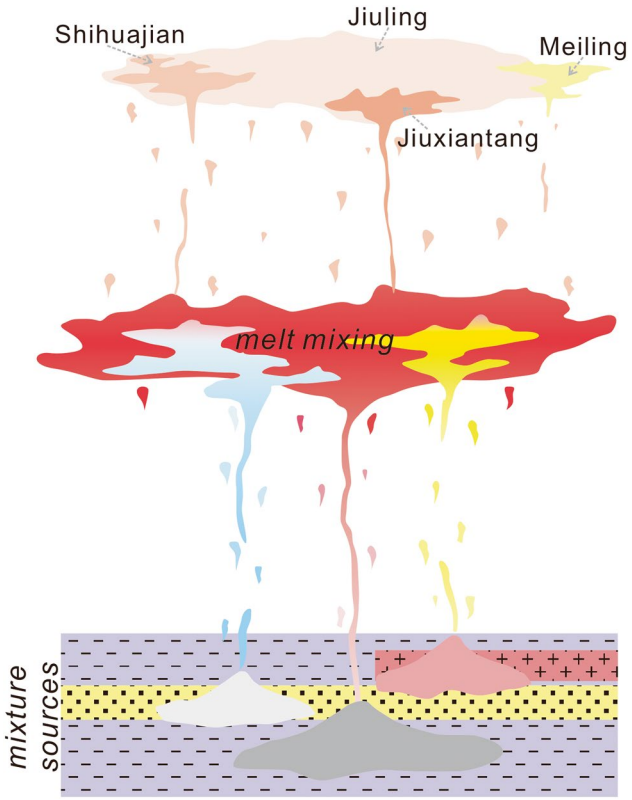

Fig. 12 A schematic model for the formation of a granitic intrusion/batholith, which involves dual mixing of heterogeneous magma sources and multiple batches of granitic melts

Conclusions

1. Peraluminous crustally derived Neoproterozoic intrusions record the incremental formation of the composite Jiuling batholith.
2. The Neoproterozoic granitoids within the batholith were predominantly derived from underlying supracrustal material that was geochemically similar to the sediments of SQS Group, combined with minor amounts of arc-related granitoid material. However, the temporal transition from the early to late stages of batholith formation also record several geochemical transitions: (1) from K-rich to Na-rich components; (2) from high to low Rb/Sr ratios; (3) from high to low zircon $\delta^{18}O$ values; and (4) from low to high $\varepsilon_{Hf}(t)$ values at given $\varepsilon_{Nd}(t)$ values. The presence of large inter-intrusion variations provides evidence of the involvement of magmas from multiple different sources. Inter-sample zircon Hf and O isotope variations also provide evidence of the mixing of multiple batches of melt within a single intrusion, with these geochemically distinct batches generated by disequilibrium melting. This dual mixing, involving heterogeneous magma sources and multiple batches of granitic melts (Fig. 12), represents the key process in the generation of the composite peraluminous batholith, and may also explain some of the geochemical diversity present within crustally derived granitoids.
3. The Neoproterozoic intrusions of the composite Jiuling batholith contain Nd–Hf isotopes that plot above the ter-

restrial array and close to the seawater array. This Nd–Hf decoupling suggests that the intrusions that formed the batholith were derived from a source containing marine sediments.

Acknowledgements This work was substantially supported by the National Natural Science Foundation of China (Grant Nos. 41802051 and 41222016). We thank the assistance from L. S. Li for analyzing geochemical data, G. C. Wang and B. Wu for LA-ICP-MS analyses, and T. Yang for zircon Hf isotope analyses.

References

Albarède F, Simonetti A, Vervoort JD, Blichert-Toft J, Abouchami W (1998) A Hf-Nd isotopic correlation in ferromanganese nodules. Geophys Res Lett 25(20):3895–3898

Appleby SK, Gillespie MR, Graham CM, Hinton RW, Oliver GJ, Kelly NM (2010) Do S-type granites commonly sample infracrustal sources? New results from an integrated O, U-Pb and Hf isotope study of zircon. Contrib Mineral Petrol 160(1):115–132

Ballouard C, Poujol M, Boulvais P, Branquet Y, Tartèse R, Vigneresse JL (2016) Nb–Ta fractionation in peraluminous granites: a marker of the magmatic-hydrothermal transition. Geology 44:231–234

Barbarin B (2005) Mafic magmatic enclaves and mafic rocks associated with some granitoids of the central Sierra Nevada batholith, California: nature, origin, and relations with the hosts. Lithos 80:155–177

Bateman PC (1992) Plutonism in the central part of the Sierra Nevada Batholith. U.S. US Government Printing Office, Washington, California

Belousova EA, Griffin WL, O'Reilly SY (2006) Zircon crystal morphology, trace element signatures and Hf isotope composition as a tool for petrogenetic modelling: examples from eastern Australian granitoids. J Petrol 47:329–353

BGMRJX (Bureau of geology and Mineral Resources of Jiangxi Province) (1984) Regional geology of Jiangxi Province. Geological Publishing House, Beijing (in Chinese with English abstract)

Boehnke P, Watson EB, Trail D, Harrison TM, Schmitt AK (2013) Zircon saturation re-revisited. Chem Geol 351:324–334

Camilletti G, Otamendi J, Tibaldi A, Cristofolini E, Leisen M, Romero R et al (2020) Geology, petrology and geochronology of sierra Valle Fértil-La Huerta batholith: implications for the construction of a middle-crust magmatic-arc section. J South Am Earth Sci 97:102423

Carpentier M, Chauvel C, Maury RC, Mattielli N (2009) The 'zircon effect' as recorded by the chemical and Hf isotopic compositions of lesser Antilles forearc sediments. Earth Planet Sci Lett 287(1):86–99

Chambers M, Memeti V, Eddy MP, Schoene B (2020) Half a million years of magmatic history recorded in a K-feldspar megacryst of the Tuolumne intrusive complex. Geology, California, USA. https://doi.org/10.1130/G46873.1

Charvet J (2013) The Neoproterozoic–early Paleozoic tectonic evolution of the South China Block: an overview. J Asian Earth Sci 74:198–209

Chen JF, Jahn BM (1998) Crustal evolution of southeastern China: evidence from Sr, Nd and Pb isotopic compositions of granitoids and sedimentary rocks. Tectonophysics 284:101–133

Chen Z, Xing G, Guo K et al (2009) Petrogenesis of keratophyes in the Pingshui group, Zhejiang: constraints from zircon U-Pb ages and Hf isotopes. Chin Sci Bull 54:1570–1578

Clarke DB (1992) Granitoid rocks. Chapman and Hall, London

Clemens JC, Regmi K, Nicholls IA, Weinberg R, Maas R (2016) The Tynong pluton, its mafic synplutonic sheets and igneous microgranular enclaves: the nature of the mantle connection in I-type granitic magmas. Contrib Miner Petrol 171:35

Coleman DS, Gray W, Glazner AF (2004) Rethinking the emplacement and evolution of zoned plutons: geochronologic evidence for incremental assembly of the Tuolumne Intrusive Suite, California. Geology 32:433–436

Collins WJ, Huang HQ, Jiang X (2016) Water-fluxed crustal melting produces Cordilleran batholiths. Geology 44(2):143–146

Couzinié S, Laurent O, Poujol M et al (2017) Cadomian S-type granites as basement rocks of the Variscan belt (Massif Central, France): implications for the crustal evolution of the north Gondwana margin. Lithos 286:16–34

Dong SW, Zhang YQ, Gao R, Su JB, Liu M, Li JH (2015) A possible buried Paleoproterozoic collisional orogen beneath central South China: evidence from seismic-reflection profiling. Precam Res 264:1–10

Farina F, Stevens G, Gerdes A, Frei D (2014) Small-scale Hf isotopic variability in the Peninsula pluton (South Africa): the processes that control inheritance of source $^{176}Hf/^{177}Hf$ diversity in S-type granites. Contrib Mineral Petrol 168:1065

Farner MJ, Lee CTA, Putirka KD (2014) Mafic–felsic magma mixing limited by reactive processes: a case study of biotite-rich rinds on mafic enclaves. Earth Planet Sci Lett 393:49–59

Fiannacca P, Williams IS, Cirrincione R (2017) Timescales and mechanisms of batholith construction: constraints from zircon oxygen isotopes and geochronology of the late Variscan Serre Batholith (Calabria, southern Italy). Lithos 277:302–314

Gao JF, Lu JJ, Lai MY, Lin YP, Pu W (2003) Analysis of trace elements in rock samples using HR-ICPMS. J Nanjing Univ (Natural Sci) 39:844–850 (in Chinese with English abstract)

Gao LZ, Yang MG, Ding XZ, Liu XY, Liu X, Lin LH, Zhang CH (2008) New SHRIMP U-Pb dating for the Shuangqiaoshan Group in South China. Geol Bull China 27(10):1744–1751 (in Chinese with English abstract)

Glazner AF, Bartley JM, Coleman DS, Gray W, Taylor ZT (2004) Are plutons assembled over millions of years by amalgamation from small magma chambers? GSA Today 14:4–11

Griffin WL, Pearson NJ, Belousova E, Jackson SE, van Achterbergh E, O'Reilly SY, Shee SR (2000) The Hf isotope composition of cratonic mantle: LAM-MC-ICPMS analysis of zircon megacrysts in kimberlites. Geochim Cosmochim Acta 64:133–147

Griffin WL, Wang X, Jackson SE, Pearson SE, O'Reilly SY, Xu XS, Zhou XM (2002) Zircon chemistry and magma genesis, SE China: in-situ analysis of Hf isotopes, Tonglu and Pingtan igneous complexes. Lithos 61:237–269

Harrison TM, Watson EB, Aikman AB (2007) Temperature spectra of zircon crystallization in plutonic rocks. Geology 35:635–638

Hofmann AE, Baker MB, Eiller JM (2014) Sub-micron-scale trace-element distributions in natural zircons of known provenance implications for Ti-in-zircon thermometry. Contrib Mineral Petrol 168:1–21

Huang XB, Yu ZZ, Zhou G (2003) Sedimentary features of the Mesoproterozoic Shuangqiaoshan group in northwestern Jiangxi. Geol Bull China 22(1):43–49

Huang H, Niu Y, Mo X (2017) Garnet effect on Nd–Hf isotope decoupling: evidence from the Jinfosi batholith, Northern Tibetan Plateau. Lithos 274:31–38

Huang H, Niu Y, Teng FZ, Wang SJ (2019) Discrepancy between bulk-rock and zircon Hf isotopes accompanying Nd–Hf isotope decoupling. Geochim Cosmochim Acta 259:17–36

Irber W (1999) The lanthanide tetrad effect and its correlation with K/Rb, Eu/Eu*, Sr/Eu, Y/Ho, and Zr/Hf of evolving peraluminous granite suites. Geochim Cosmochim Acta 63:489–508

Jackson SE, Pearson NJ, Griffin WL, Belousova EA (2004) The application of laser ablation-inductively coupled plasma-mass spectrometry to in situ U-Pb zircon geochronology. Chem Geol 211:47–69

Janney PE, Leroex AP, Carlson RW (2005) Hafnium Isotope and trace element constraints on the nature of mantle heterogeneity beneath the central southwest Indian Ridge (13°E–47°E). J Petrol 46(12):2427–2464

Kemp AIS, Hawkesworth CJ, Foster GL, Paterson BA, Woodhead JD, Hergt JM, Gray CM, Whitehouse MJ (2007) Magmatic and crustal differentiation history of granitic rocks from Hf-O isotopes in zircon. Science 315:980–983

Laumonier M, Scaillet B, Pichavant M, Champallier R, Andujar J, Arbaret L (2014) On the conditions of magma mixing and its bearing on andesite production in the crust. Nat Commun 5(1):1–12

Laurent O, Zeh A, Gerdes A, Villaros A, Gros K, Słaby E (2017) How do granitoid magmas mix with each other? Insights from textures, trace element and Sr–Nd isotopic composition of apatite and titanite from the Matok pluton (South Africa). Contrib Miner Petrol 172:80

Li XH, Li ZX, Ge WC, Zhou HW, Li WX, Liu Y, Wingate MTD (2003) Neoproterozoic granitoids in South China: crustal melting above a mantle plume at *ca.* 825Ma? Precambrian Res 122:45–83

Li JY, Wang XL, Zhang FF, Zhou XH, Shu XJ (2016) A rhythmic source change of the Neoproterozoic basement meta-sedimentary sequences in the Jiangnan Orogen: implications for tectonic evolution on the southeastern margin of the Yangtze Block. Precambrian Res 280:46–60

Marsh BD (2015) Magmatism, magma, and magma chambers. In: Watts AB (ed) Crustal and lithosphere dynamics. Elsevier, Amsterdam, pp 276–333

Michel J, Baumgartner L, Putlitz B, Schaltegger U, Ovtcharova M (2008) Incremental growth of the Patagonian Torres del Paine laccolith over 90 ky. Geology 36:459–465

Miller CF, McDowell SM, Mapes RW (2003) Hot and cold granites? Implications of zircon saturation temperatures and preservation of inheritance. Geology 31:529–532

Miller JS, Matzel JEP, Miller CF, Burgess SD, Miller RB (2007) Zircon growth and recycling during the assembly of large, composite plutons. J Volcanol Geotherm Res 167:282–299

Miller CF, Furbish DJ, Walker BA, Claiborne LL, Koteas GC, Bleick HA, Miller JS (2011) Growth of plutons by incremental emplacement of sheets in crystal-rich host: evidence from Miocene intrusions of the Colorado River region, Nevada, USA. Tectonophysics 500:65–77

Moyen JF, Laurent O (2018) Archaean tectonic systems: a view from igneous rocks. Lithos 302–303:99–125

Moyen JF, Laurent O, Chelle-Michou C, Couzinié S, Vanderhaeghe O, Zeh A, Villaros A, Gardien V (2017) Collision vs. subduction-related magmatism: two contrasting ways of granite formation and implications for crustal growth. Lithos 277:154–177

Nikkilä K, Mänttäri I, Nironen M, Eklund O, Korja A (2016) Three stages to form a large batholith after terrane accretion—an example from the Svecofennian orogen. Precambrian Res 281:618–638

Patchett PJ, White WM, Feldmann H, Kielinczuk S, Hofmann AW (1984) Hafnium rare-earth element fractionation in the sedimentary system and crustal recycling into the Earth's mantle. Earth Planet Sci Lett 69:365–378

Petford N, Cruden AR, McCaffrey KJW, Vigneresse JL (2000) Granite magma formation, transport and emplacement in the Earth's crust. Nature 408:669–673

Polat A, Münker C (2004) Hf–Nd isotope evidence for contemporaneous subduction processes in the source of late Archean arc lavas from the Superior Province, Canada. Chem Geol 213:403–429

Rong W, Zhang SB, Zheng YF (2017) Back-reaction of Peritectic Garnet as an explanation for the origin of Mafic enclaves in S-type granite from the Jiuling Batholith in South China. J Pet 58(3):569–598

Rong W, Zhang SB, Zheng YF, Gao P (2018) Mixing of felsic magmas in granite petrogenesis: geochemical records of zircon and garnet in peraluminous granitoids from South China. J Geophys Res-Sol Ea 123(4):2738–2769

Rudnick RL, Gao S (2003) Composition of the continental crust. In: Rudnick RL, Holland HD, Turekian KK (eds) Treatise on geochemistry, the crust, vol 3. Elsevier, Amsterdam, pp 1–64

Ruprecht P, Bachmann O (2010) Pre-eruptive reheating during magma mixing at Quizapu volcano and the implications for the explosiveness of silicic arc volcanoes. Geology 38(10):919–922

Schmitz MD, Vervoort JD, Bowring SA, Patchett PJ (2004) Decoupling of the Lu–Hf and Sm–Nd isotope systems during the evolution of granulitic lower crust beneath southern Africa. Geology 32(5):405–408

Stichel T, Frank M, Rickli J, Haley BA (2012) Hafnium and neodymium isotope composition of seawater in the Atlantic sector of the Southern Ocean. Earth Planet Sci Lett 317–318:282–294

Tang M, Wang XL, Shu XJ, Wang D, Yang T (2014) Hafnium isotopic heterogeneity in zircons from granitic rocks: geochemical evaluation and modeling on "zircon effect" in crustal anatexis. Earth Planet Sci Lett 389:188–199

Tichomirowa M, Kässner A, Sperner B, Lapp M, Leonhardt D, Linnemann U et al (2019) Dating multiply overprinted granites: The effect of protracted magmatism and fluid flow on dating systems (zircon U-Pb: SHRIMP/SIMS, LA-ICP-MS, CA-ID-TIMS; and Rb–Sr, Ar–Ar)–granites from the Western Erzgebirge (Bohemian Massif, Germany). Chem Geol 519:11–38

Valley JW (2003) Oxygen isotopes in zircon. Rev Mineral Geochem 53(1):343–385

Valley JW, Lackey JS, Cavosie AJ, Clechenko CC, Spicuzza MJ, Basei MAS et al (2005) 44 Billion years of crustal maturation: oxygen isotope ratios of magmatic zircon. Contrib Mineral Petrol 150(6):561–580

Van de Flierdt T, Goldstein SL, Hemming SR, Roy M, Frank M, Halliday AN (2007) Global neodymium–hafnium isotope systematics—revisited. Earth Planet Sci Lett 259(3–4):432–441

Vervoort JD, Blichert-toft J (1999) Evolution of the depleted mantle: Hf isotope evidence from juvenile rocks through time. Geochim Cosmochim Acta 63:533–556

Vervoort JD, Patchett PJ (1996) Behavior of hafnium and neodymium isotopes in the crust: constraints from Precambrian crustally derived granites. Geochim Cosmochim Acta 60:3717–3733

Vervoort JD, Patchett PJ, Blichert-Toft J, Albarède F (1999) Relationships between Lu–Hf and Sm–Nd isotopic systems in the global sedimentary system. Earth Planet Sci Lett 168:79–99

Vervoort JD, Patchett PJ, Albarède F, Blichert-Toft J, Rudnick R, Downes H (2000) Hf–Nd isotopic evolution of the lower crust. Earth Planet Sci Lett 181:115–129

Vervoort JD, Plank T, Prytulak J (2011) The Hf–Nd isotopic composition of marine sediments. Geochim Cosmochim Acta 75:5903–5926

Villaros A, Buick IS, Stevens G (2012) Isotopic variations in S-type granites: an inheritance from a heterogeneous source? Contrib Mineral Petrol 163:243–257

Walker BA Jr, Miller CF, Claiborne LE, Wooden JL, Miller JS (2007) Geology and geochronology of the Spirit Mountain batholith, southern Nevada: implications for timescales and physical processes of batholith construction. J Volcanol Geotherm Res 167:239–262

Wang XL, Zhou JC, Qiu JS, Zhang WL, Liu XM, Zhang GL (2006) LA-ICP-MS U-Pb zircon geochronology of the Neoproterozoic igneous rocks from Northern Guangxi, South China: implications for tectonic evolution. Precambrian Res 145:111–130

Wang XL, Zhou JC, Griffin WL et al (2007) Detrital zircon geochronology of Precambrian basement sequences in the Jiangnan orogen: dating the assembly of the Yangtze and Cathaysia blocks. Precambrian Res 159:117–131

Wang W, Zhou MF, Yan DP, Li JW (2012) Depositional age, provenance, and tectonic setting of the Neoproterozoic Sibao Group, southeastern Yangtze Block, South China. Precambrian Res 192:107–124

Wang D, Wang XL, Zhou JC, Shu XJ (2013) Unraveling the Precambrian crustal evolution by Neoproterozoic conglomerates, Jiangnan orogen: U-Pb and Hf isotopes of detrital zircons. Precambrian Res 233:233–236

Wang W, Zhou MF, Yan DP, Li L, Malpas J (2013) Detrital zircon record of Neoproterozoic active-margin sedimentation in the eastern Jiangnan Orogen, South China. Precambrian Res 235:1–19

Wang XL, Zhou JC, Wan YS, Kitajima K, Wang D, Bonamici C, Qiu JS, Sun T (2013) Magmatic evolution and crustal recycling for Neoproterozoic strongly peraluminous granitoids from southern China: Hf and O isotopes in zircon. Earth Planet Sci Lett 366:71–82

Wang XL, Zhou JC, Griffin WL et al (2014) Geochemical zonation across a Neoproterozoic Orogenic belt: isotopic evidence from granitoids and Metasedimentary rocks of the Jiangnan Orogen, China. Precambrian Res 242:154–171

Wang D, Wang XL, Cai Y, Chen X, Zhang FR, Zhang FF (2017) Heterogeneous conservation of zircon xenocrysts in late jurassic granitic intrusions within the Neoproterozoic Jiuling Batholith, South China: a magma chamber growth model in deep crustal hot zones. J Petrol 58(9):1781–1810

Wang D, Wang XL, Cai Y, Goldstein SL, Yang T (2018) Do Hf isotopes in magmatic zircons represent those of their host rocks? J Asian Earth Sci 154:202–212

Watson EB, Harrison TM (2005) Zircon thermometer reveals minimum melting conditions on earliest Earth. Science 308:841–844

Wiedenbeck M, Alle P, Corfu F, Griffin WL, Meier M, Oberli F, von Quadt A, Roddick JC, Spiegel W (1995) Three natural zircon standards for U-Th–Pb, Lu–Hf, trace element and REE analyses. Geostand Newsl 19:1–23

Woodhead JD, Hergt JM (2005) A preliminary appraisal of seven natural zircon reference materials for in situ Hf isotope determination. Geostand Geoanal Res 29:183–195

Xin Y, Li J, Dong S, Zhang Y, Wang W, Sun H (2017) Neoproterozoic post-collisional extension of the central Jiangnan Orogen: geochemical, geochronological, and Lu–Hf isotopic constraints from the *ca.* 820–800 Ma magmatic rocks. Precambrian Res 294:91–110

Yang JH, Wu FY, Wilde SA, Xie LW, Yang YH, Liu XM (2007) Tracing magma mixing in granite genesis: in situ U-Pb dating and Hf-isotope analysis of zircons. Contrib Mineral Petrol 153:177–190

Ye MF, Li XH, Li WX, Liu Y, Li ZX (2007) SHRIMP zircon U-Pb geochronological and whole-rock geochemical evidence for an early Neoproterozoic Sibaoan magmatic arc along the southeastern margin of the Yangtze Block. Gondwana Res 12(1–2):144–156

Yu JH, Wang L, O'Reilly SY, Griffin WL, Zhang M, Li C, Shu L (2009) A Paleoproterozoic orogeny recorded in a long-lived cratonic remnant (Wuyishan terrane), eastern Cathaysia Block, China. Precambrian Res 174:347–363

Yu JH, O'Reilly SY, Zhou MF, Griffin WL, Wang LJ (2012) U-Pb geochronology and Hf–Nd isotopic geochemistry of the Badu Complex, Southeastern China: implications for the Precambrian crustal evolution and paleogeography of the Cathaysia Block. Precambrian Res 222–223:424–449

Zhang SB, Zheng YF (2013) Formation and evolution of Precambrian continental lithosphere in South China. Gondwana Res 23:1241–1260

Zhang SB, Zheng YF, Wu YB, Zhao ZF, Gao S, Wu FY (2006a) Zircon isotope evidence for ≥3.5 Ga continental crust in the Yangtze craton of China. Precambrian Res 146:16–34

Zhang SB, Zheng YF, Wu YB, Zhao ZF, Gao S, Wu FY (2006b) Zircon U-Pb age and Hf–O isotope evidence for Paleoproterozoic metamorphic event in South China. Precambrian Res 151:265–288

Zhao JH, Zhou MF, Zheng JP (2013) Constraints from zircon U-Pb ages, O and Hf isotopic compositions on the origin of Neoproterozoic peraluminous granitoids from the Jiangnan Fold Belt, South China. Contrib Mineral Petrol 166:1505–1519

Zheng YF, Zhang SB, Zhao ZF, Wu YB, Li X, Li Z, Wu FY (2007) Contrasting zircon Hf and O isotopes in the two episodes of Neoproterozoic granitoids in South China: implications for growth and reworking of continental crust. Lithos 96:127–150

Zhong YF, Ma CQ, She ZB, Lin GC, Xu HJ, Wang RJ, Yang KG, Liu Q (2005) SHRIMP U-Pb Zircon Geochronology of the Jiuling Granitic Complex Batholith in Jiangxi Province. Earth Sci–J China Univ Geosci 30:685–691 (in Chinese with English Abstract)

Zhou MF, Yan DP, Kennedy AK, Li Y, Ding J (2002) SHRIMP U-Pb zircon geochronological and geochemical evidence for Neoproterozoic arc-magmatism along the western margin of the Yangtze Block, South China. Earth Planet Sci Lett 196:51–67